Picosecond Optical Sampling of GaAs Integrated Circuits

KURT J. WEINGARTEN, STUDENT MEMBER, IEEE, MARK J. W. RODWELL, AND DAVID M. BLOOM, FELLOW, IEEE

(Invited Paper)

Abstract—**Direct electrooptic sampling is a noncontact optical probing technique for measuring with picosecond time resolution the voltage waveforms at internal nodes within GaAs integrated circuits. The factors contributing to system bandwidth, sensitivity, spatial resolution, and circuit perturbation are discussed, as are the circuit requirements for realistic testing of analog and digital devices. Measurements of high-speed GaAs integrated circuits are presented, including time-domain waveform and timing measurements of digital and analog circuits and frequency-domain transfer function measurements of microwave circuits and transmission structures.**

I. Introduction

THE development of advanced GaAs devices and integrated circuits has been spurred by a number of applications, including microwave and millimeter-wave radar and communication systems, fiber optical digital data transmission at gigahertz rates, high-speed data aquisition, and the constant push for faster digital logic in high-speed computers and signal processors; the IC's developed for these applications are creating new demands upon high-speed electronic instrumentation.

One demand is for increased instrument bandwidth. GaAs MESFET's have demonstrated a maximum frequency of oscillation, f_{max}, in excess of 110 GHz [1], while pseudomorphic InGaAs/AlGaAs modulation-doped field-effect transistors [2] have shown power-gain bandwidth products which extrapolate to give $f_{max} \approx 200$ GHz, resonant tunneling diodes have oscillated at 56 GHz [3], and heterojunction bipolar transistors and permeable base transistors currently under development should show similar performance. Because the maximum frequency of oscillation of these devices is often greater than the 100 GHz bandwidth of commercial millimeter-wave network analyzers, f_{max} is estimated by extrapolation from measurements at lower frequencies. Used as switching elements, propagation delays and transition times of 1–10 ps should be expected for these devices, well below the resolution of commercial sampling oscilloscopes. In either case the device bandwidth exceeds that of the measurement instrument.

A second demand is for noninvasive access to the internal signals within high-speed integrated circuits. GaAs digital integrated circuits of MSI (medium-scale integration) complexity and 1–5 GHz clock rates are now available commercially, as are GaAs monolithic microwave integrated circuits (MMIC's) of SSI (small-scale integration) complexity and 1-26 GHz bandwidths. More complex LSI (large-scale integration) digital circuits are under development, and experimental SSI digital circuits operating with 18 GHz clock rates [4] have been demonstrated. In contrast to silicon LSI integrated circuits opearing at clock rates in the tens and hundreds of megahertz, the development of GaAs high-speed circuits is hampered both by poorly-refined device models and by layout-dependent circuit parasitics associated with the high frequencies of operation. A test instrument providing noninvasive measurements within the integrated circuit would permit full characterization of such complex high-speed IC's.

These issues have motivated a number of researchers to investigate alternative test techniques, both to increase measurement bandwidth and to allow internal testing of IC's. This paper begins with a review of conventional test methods and instruments, summarizes several new test techniques for IC's, and then describes in detail the principles, capabilities, and IC measurement results of direct electrooptic sampling, a measurement technique that allows for internal-node voltage measurements in GaAs IC's with picosecond time resolution, corresponding to bandwidths in excess of 100 GHz.

A. Electrical Test Methods

We begin by considering the limitations of conventional test instruments. Their capabilities and characteristics are determined by two features—the IC probe that connects the test instrument to the circuit and the test instrument itself. The IC probe has its own intrinsic bandwidth that may limit the test method. In addition, the probe also determines an instrument's ability to probe *internal* to the IC due to its size (limiting its spatial resolution) and influence on circuit performance (loading of

Manuscript received June 3, 1987; revised September 4, 1987. This work was supported in part by the Air Force Office of Scientific Research under Grant F49620-84-K-0139, by the Joint Services Electronic Program under Grant N00014-K-0327, and by the Wright-Patterson Air Force Base Avionics Laboratory under Contract F33615-86-C-1126. The work of K. J. Weingarten was supported in part by a Newport Research Award. The work of M. J. W. Rodwell was supported in part by an IBM Pre-Doctoral Fellowship.

The authors are with the Edward L. Ginzton Laboratory, Stanford University, Stanford, CA 94305.

IEEE Log Number 8717851.

the circuit from its characteristic and parasitic impedances.) The test instrument sets the available bandwidth given perfect IC probes or packaged circuits, and defines the type of electric test, such as measuring time or frequency response.

Connection of a test instrument to an IC begins with the external connectors, such as the 50 Ω coaxial K-connector or the APC-2.4, new connectors for 46 GHz (K), or 50 GHz (APC 2.4) operation. The IC probes are the *transitions* from the coaxial cable to some type of contact point with a size comparable to an IC bond pad. Low-frequency signals are often connected with needle probes. At frequencies greater than several hundred megahertz these probes have serious *parasitic* impedances, due to shunt capacitance from fringing fields and series inductance from the long, thin needle. The parasitic impedances and the relatively large probe size compared to IC interconnects limit their effective use to low-frequency external input or output circuit responses at the bond pads. For signals greater than several hundred megahertz, the recently developed Cascade Microtech probe [5], [6] has demonstrated IC connections to millimeter-wave frequencies of 50 GHz. The probe consists of a coaxial connector with a transition to 50 Ω coplanar waveguide (CPW) transmission line that then tapers to bond pad size contacts. They offer good microwave performance, but their size limits test points to IC bond pads and their 50 Ω characteristic impedance limits their use to input or output sections of the IC.

Thus, electrical probes suffer from a measurement dilemma. Good high-frequency probes use transmission lines to control the line impedance from the coaxial transition to the IC bond pad and to reduce parasitic impedances. The low characteristic impedance of such lines (typically 50 Ω) limits their use to input/output connections. High-impedance probes suitable for probing intermediate circuit nodes have significant parasitic impedances at microwave frequencies, severely perturbing the circuit operation and affecting the measurement accuracy. In both cases, the probe size is large compared to IC interconnect size, limiting their use to test points the size of bond pads.

Conventional test instruments for measuring high-speed electrical signals consist of sampling oscilloscopes, spectrum analyzers, and network analyzers. Sampling oscilloscopes measure the time response of repetitive signals with a resolution as short as 25 ps or a bandwidth of 14 GHz. Combined with transmission line probes this instrument gives either time domain reflectometry measurements or signal waveforms of an IC's external response, but has neither the time resolution required for state-of-the-art GaAs IC's nor the ability to measure the internal node response of MSI or LSI IC's. A promising note is the recent introduction of a new sampling oscilloscope based on Josephson Junction superconducting technology [7] with a time resolution of about 8 ps. As with slower sampling oscilloscopes, however, the 50 Ω connectors limit its use to external characterization of IC's.

Spectrum and network analyzers measure the response of circuits in the frequency domain, with a range of 26.5 GHz typically and limited extension through millimeter-wave frequencies to 300 GHz. A spectrum analyzer measures the power spectrum of a signal, while network analyzers measure the vector transfer function (magnitude and phase) of a network as a function of frequency. The small-signal, linear characteristics of microwave devices and circuits measured with a network analyzer are usually expressed in terms of the scattering parameters. These provide a measure (often extrapolated) of f_{max}, a device's maximum frequency of oscillation, and f_τ, the unity current gain frequency, figures of merit of a device's operation speed. The frequency range of these instruments can be extended to millimeter-wave frequencies (300 GHz for the spectrum analyzer, 100 GHz for the network analyzer) using external source multipliers, mixers, and waveguide connectors, but the frequency coverage is limited to 1.5 : 1 waveguide bandwidths and the waveguide connectors require a hybrid mount of the IC in a waveguide package, preventing wafer testing of the IC. Network analyzers can provide time-domain measurements of a network's small-signal step or impulse response by Fourier transforming the small-signal frequency-domain two-port device parameters. For large-signal measurements, where the network is no longer linear, the principle of superposition cannot be applied, preventing calculation of the large-signal time-domain response from measurements of frequency-domain transfer functions. For example, the network analyzer cannot measure the time waveform response of the IC's due to amplifier saturation. Although spectrum analyzers can measure the harmonic spectrum magnitude of saturated or large-signal circuit responses, the phases of the harmonics are not measured, and the large-signal time waveforms again cannot be inferred. Both instruments also rely on 50 Ω connectors and IC probes, limiting their ability to probe an IC to its external response. For network analysis, a further issue is deembedding the device parameters from the connector and circuit fixture response, a task which grows progressively more difficult at increasing frequencies, particularly for millimeter-wave testing.

B. Nonelectrical, Novel Test Techniques

With the objective of either increased bandwidth or internal IC testing with high spatial resolution (or both) a number of new test techniques have been introduced and demonstrated. One method of measuring a voltage on IC conductors is to energy analyze secondary electron emission. To test logic level signals in VLSI silicon IC's researchers in the late 1960's developed the voltage contrast scanning electron microscope (SEM) or E-beam probing [8], [9]. This technique uses an electron beam from an SEM to stimulate secondary electron emission from surface metallization. For a metal conductor at ground or negative potential, the electrons have sufficient energy to be collected by a detector shielded by an energy analyzer grid. Metal lines at a positive potential retard the emitted electrons, lowering their energy and reducing the number of electrons detected. The detected signal is small for IC

voltage levels; to improve time resolution the signal is sampled with electron beam pulses and averaged to improve signal-to-noise ratio.

Commercial SEM's have sensitivities of 1–10 mV, bandwidths up to 2 GHz or time resolutions of ≈ 200 ps, and a spatial resolution as small as 20 nm. Compared to typical operating speeds of commercial silicon VLSI (clock rates of 10–100 MHz) this technique has good time resolution, acceptable sensitivity, and excellent spatial resolution. The system's time resolution is set by gating the E-beam from the thermionic cathodes of standard SEM's. For decreasing electron beam duration required for increased time resolution, the average beam current decreases, degrading measurement sensitivity and limiting practical systems to a time resolution of several hundred picoseconds. To overcome this limitation, a technique which implements a photocathode triggered by an intense picosecond optical pulse to generate short, high-current electron pulses [10] has been demonstrated. This approach shows promise for achieving time resolution below 10 ps with the SEM probe. The major drawbacks of SEM testing are its complexity and its relatively high cost.

Photoemissive sampling, based on analyzing secondary electron emission from IC conductors similar to E-beam testing, uses intense, energetic light from a pulsed picosecond laser focused on an IC conductor to generate photoelectrons. An extraction/retarding grid combination placed in close proximity to the conductor energy analyzes the electrons, with a resulting secondary electron emission varying with the conductor potential. The feasibility of this new approach is made possible by picosecond pulsewidth, high peak power lasers, and offers a potential improvement in time resolution and sensitivity over the SEM probe. The technique is not available commercially, but a number of researchers have demonstrated systems with time resolution as short as 7 ps with good spatial resolution and millivolt sensitivity [11]–[13]. With both electron-beam and photoemissive sampling, electron beams and electron extraction fields can produce charge concentrations within the semiconductor substrate through charging of deep levels, or at its surface, through field-induced surface inversion.

A technique which optically senses free-carrier charge density was recently developed for measurements within silicon IC devices [14], [15]. Because of its centrosymmetric crystal structure, silicon exhibits no bulk second-order optical nonlinearities, such as the electrooptic effect, to use as a basis for an optical measurement system. Third-order effects, such as voltage-dependent second-harmonic generation or the optical Kerr effect, are in general very weak and result in impractical systems in terms of measurement sensitivity and implementation. Most semiconductor devices function by modulating charge density within a control region, which contributes to material index of refraction as described by the plasma-optical relation

$$n = n_0\left(1 - \frac{\omega_p^2}{\omega^2}\right)^{1/2} \tag{1}$$

$$\omega_p^2 = \frac{q^2 N}{\epsilon_s m_e^*} + \frac{q^2 P}{\epsilon_s m_h^*} \tag{2}$$

where n_0 is the bulk index of refraction, ω is the optical probe frequency, ω_p is the plasma resonance frequency, N is the electron concentration in the conduction band, P is the hole concentration in the valence band, ϵ_s is the permittivity of the substrate material, and m_e^* and m_h^* are the electron/hole conductivity effective masses. The change in charge density is detected with a compact optical interferometer using a 1.3 μm wavelength (the absorption minimum in silicon) semiconductor laser as the probe, shown schematically in Fig. 1. In contrast to electrooptic techniques, where typical probe beam intensity modulation is on the order of 0.1 percent, the charge density typical of integrated silicon bipolar transistors results in probe beam modulation in the charge-sensing system on the order of 1 percent. This sensitivity has allowed the demonstration of single-shot (i.e., no repetitive sampling) detection of a silicon bipolar junction transistor's switching signal in a 200 MHz bandwidth (Fig. 2). Since the plasma-optical effect occurs in all semiconductor materials, this technique is applicable to GaAs IC's and shows promise for studying device characteristics and charge dynamics.

Another optical probe scheme is electrooptic sampling, which uses an electrooptic light modulator to intensity modulate a probe beam in proportion to a circuit voltage. The technique was initially developed to measure the response of photoconductors and photodetectors faster than the time resolution of sampling oscilloscopes [16]–[19] and used an external electrooptic modulator (typically lithium tantalate, $LiTaO_3$) connected to the device under test. A polarized optical probe beam passes through an electrooptic crystal, whose index of refraction changes due to the presence of an electrical signal (Fig. 3). The polarization of the light after passing through the electrooptic crystal depends on the signal driving modulator, and passing the probe beam through a polarizer results in a signal-dependent intensity modulation. The approach exhibits excellent time resolution (< 0.5 ps) due to the advanced level of ultrashort pulse generation with the colliding-pulse mode-locked (CPM) laser and the very high intrinsic speed of the electrooptic effect. Combined with a cryogenic system, optical measurements of electrical signals have been made at liquid helium temperatures [20]. However, the hybrid lithium tantalate electrooptic modulator requires connecting the test point on the IC to the transmission line of the modulator, restricting its use to external test points. Unless carefully designed, the system's time resolution is degraded by the hybrid connection between the modulator and the device under test, due to the loading of the test point from the relatively low characteristic impedance of the transmission line, and due to the parasitic impedances of bond wires.

Using an electrooptic needle probe (Figs. 4 and 5) [21], the technique has been extended to internal node probing of IC's. The needle, a fused silica rod with a 40 $\times$ 40 micron tip of $LiTaO_3$ coated for high reflection of the

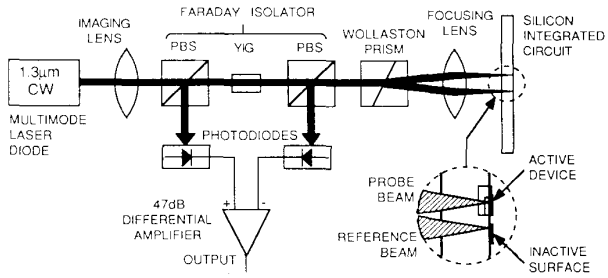

Fig. 1. Charge-sensing system schematic [14], [15]. The Wollaston prism separates the input beam into a probe beam and a reference beam. The presence of charge in the probe beam path results in a change in output intensity at the photodiodes proportional to the charge concentration, as described in the text. PBS denotes a polarizing beamsplitter cube.

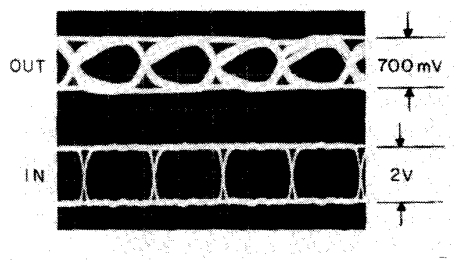

Fig. 2. Eye diagram of the stored base charge in a silicon bipolar-junction transistor, as monitored by the optical charge-sensing system, upper trace. The corresponding base voltage is shown in the lower trace. The input signal is 25 MBd pseudorandom Manchester-coded data. Time scale is 20 ns/div.

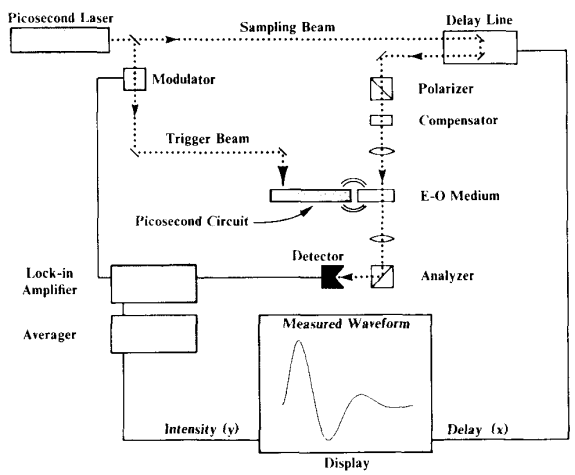

Fig. 3. Electrooptic sampling system [18]. Courtesy of J.A. Valdmanis, AT&T Bell Laboratories.

probe beam, is brought close to a conductor, introducing fields within the probe tip. As with the hybrid electrooptic scheme, the electric fields change the polarization of the probing beam, and the reflected beam is analyzed by a polarizer. The $LiTaO_3$ electrooptic material, transparent to visible wavelength light, allows the use of ultrashort sampling pulses from a CPM laser; a step response rise-time of less than 300 fs has been demonstrated [22], [23].

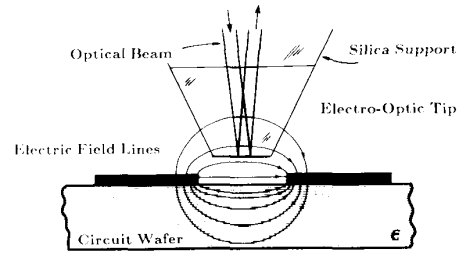

Fig. 4. Electrooptic needle probe for on-wafer measurements [21], [22]. Courtesy of J. A. Valdmanis, AT&T Bell Laboratories.

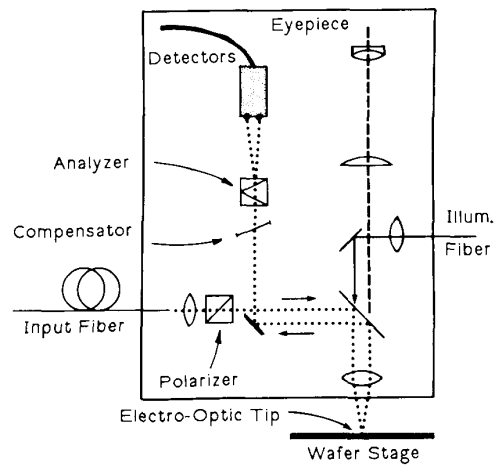

Fig. 5. Sampling system for on-wafer measurements with the electrooptic needle probe. Courtesy of J. A. Valdmanis, AT&T Bell Laboratories.

Because the probe relies on no optical or electrical properties of the circuit under test, circuits of any substrate material can be tested without sample preparation. The probe exhibits some small circuit invasiveness through capacitive loading on the order of 10 femtofarads due to the proximity of the $LiTaO_3$ probe tip of dielectric constant $\epsilon_r = 40$. The polarization shift in lithium tantalate, proportional to the lateral electric field, may make the probe sensitive to signals from nearby conductors in addition to the potential of the probed conductor.

The external electrooptic sampling techniques described above can provide signal measurements with subpicosecond time resolution (equivalent to bandwidths of approaching 1 THz). Direct electrooptic sampling, a related technique where the substrate of the GaAs circuit under test serves as the electrooptic modulator, eliminates the electrical parasitics associated with external electrooptic elements and provides voltage measurements of points internal to the IC with picosecond time resolution and micron spatial resolution. This method's principles, capabilities, and circuit measurements results are described in the following sections.

II. Principles of Direct Electrooptic Sampling in GaAs IC's

The electroooptic effect, an anisotropic variation in a material's dielectric constant due to an applied electric

field, is present in a variety of noncentrosymmetric crystals. Among these are GaAs, InP, and AlAs, used for high-speed semiconductor devices, and lithium niobate ($LiNbO_3$), lithium tantalate ($LiTaO_3$), and potassium dihydrogen phosphate (KH_2PO_4), used for nonlinear optical devices. Centrosymmetric crystals do not exhibit the electrooptic effect; notable among these materials are silicon and germanium. The change in refractive index of electrooptic materials with electric field can be used for optical phase-modulation, and, from this, polarization-modulation or intensity-modulation [24], [25]. Direct electrooptic sampling uses the electrooptic effect in GaAs to obtain voltage-dependent intensity modulation of a probe beam [26], [27]. As with other experimental probing methods, a pulsed optical probe beam permits a potential time resolution on the order of 1 ps or instrument bandwidths greater than 100 GHz.

Without external electrooptic elements, the invasive properties of those elements are eliminated, permitting probing with no electrical contact, no loading of the test point with low-impedance transmission lines, and no parasitic probe impedance. Because the probing beam can be focused to a spot of diameter of several microns, the probe's spatial resolution allows access to finely-spaced conductors in LSI GaAs circuits. Direct electrooptic sampling thus provides the bandwidth, the spatial resolution, and the internal-node access necessary for characterization of high-speed GaAs integrated circuits.

A. Electrooptic Voltage Probing in a GaAs Crystal

GaAs is one of simplest electrooptic crystals, a zinc-blende with crystal symmetry $\bar{4}3$ m. Its cubic structure results in no natural (field-free) birefringence and a symmetric electrooptic tensor with equal-valued elements. The electrooptic tensor in GaAs is [28]

$$r_{jk} = \begin{bmatrix} 0 & 0 & 0 \\ 0 & 0 & 0 \\ 0 & 0 & 0 \\ r_{41} & 0 & 0 \\ 0 & r_{41} & 0 \\ 0 & 0 & r_{41} \end{bmatrix}. \tag{3}$$

An applied electric field induces a birefringence described by the index ellipsoid

$$\frac{x^2}{n_0^2} + \frac{y^2}{n_0^2} + \frac{z^2}{n_0^2} + 2r_{41}yzE_x + 2r_{41}xzE_y + 2r_{41}xyE_z = 1 \tag{4}$$

where n_0 is the zero-field refractive index, r_{41} is the electrooptic coefficient for GaAs, and E is the applied electric field in the direction by its subscript. The intersection of the index ellipsoid and a plane normal to the optical propagation direction defines an ellipse whose major and minor axes give the allowed (eigenvector) polarization directions and their refractive indexes.

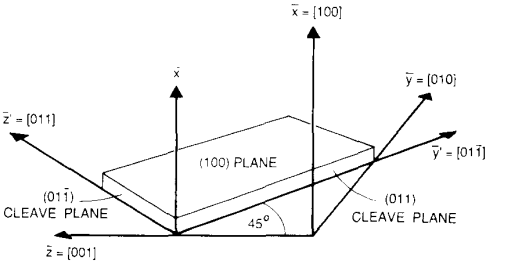

Fig. 6. Principal axes and cleave planes in (100)-cut gallium arsenide.

To relate this to an IC substrate, Fig. 6 shows the principal crystal axes of a GaAs IC fabricated on standard (100)-cut material. The ***X***, ***Y***, and ***Z*** axes are aligned with the ⟨100⟩ directions of the GaAs cubic Bravais lattice, while the ***Y'*** and ***Z'*** axes are aligned with the [01$\bar{1}$] and [011] directions parallel to the cleave planes of the a GaAs wafer (along which individual IC's are scribed) and 45° to the [010] and [001] directions. For an optical plane wave traveling in the ***X*** direction, the intersection of the index ellipsoid and the $x = 0$ plane normal to its direction of propagation defines an ellipse in the ($\boldsymbol{Y'}$, $\boldsymbol{Z'}$) plane

$$y'^2\left(\frac{1}{n_0^2} - r_{41}E_x\right) + z'^2\left(\frac{1}{n_0^2} + r_{41}E_x\right) = 1. \tag{5}$$

The ***Y'*** and ***Z'*** axes are the eigenvectors of the electrooptic effect and form the natural coordinate system for describing electrooptic sampling in GaAs IC's. The refractive indexes $n_{y'}$ and $n_{z'}$ in the ***Y'*** and ***Z'*** directions are

$$n_{y'} \approx n_0 + \frac{n_0^3 r_{41} E_x}{2} \tag{6a}$$

$$n_{z'} \approx n_0 - \frac{n_0^3 r_{41} E_x}{2} \tag{6b}$$

and these field-dependent refractive indexes result in different phase shift for beam polarizations in the ***Y'*** and ***Z'*** directions.

Consider the transmission electrooptic amplitude modulator shown in Fig. 7. A circularly-polarized plane wave propagating through the substrate receives a change in phase between the ***Y'*** and ***Z'*** polarizations due to the electrooptic effect in proportion to the electric field given by

$$\Delta\varphi = \frac{2\pi n_0^3 r_{41}}{\lambda_0} E_x W = \frac{2\pi n_0^3 r_{41}}{\lambda_0} V \tag{7}$$

such that the beam emerging from the substrate has changed from circular to slightly elliptical polarization. Note that the product $E_x W$ of the substrate thickness and the x-component of the electric field is the potential difference V between the front and back surfaces of the GaAs wafer where the probing beam traverses the wafer. This result holds for a general field distribution; a plane-wave optical beam propagating along a ⟨100⟩ direction experiences a change in phase shift proportional to product of

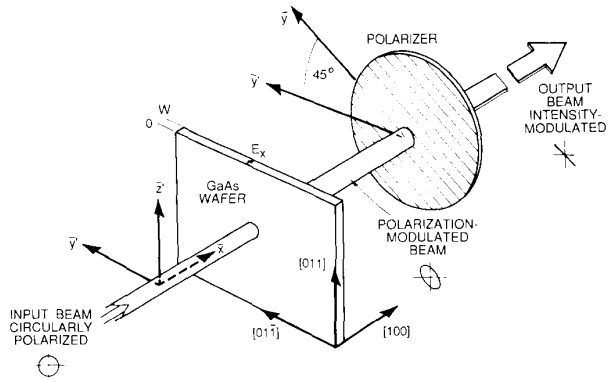

Fig. 7. Gallium arsenide electrooptic intensity modulator.

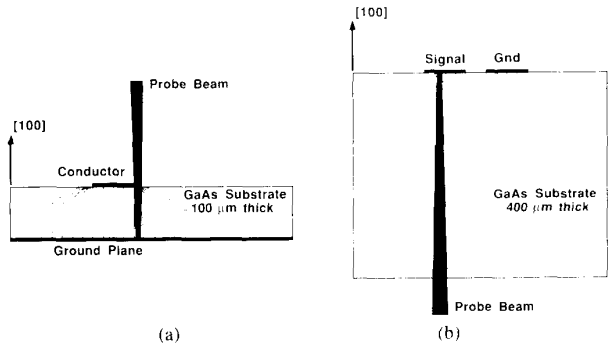

Fig. 8. Reflection-mode probing geometries for electrooptic sampling of GaAs integrated circuits. The frontside geometry is used for probing microstrip transmission lines on MMIC's, while the backside geometry is used for probing planar transmission lines on MMIC's and interconnects lines on digital IC's. (a) Frontside probing. (b) Backside probing.

the longitudinal electric field and the substrate thickness, i.e., it is *only* affected by the potential difference V across the wafer at the probe point.

To measure this voltage-induced polarization change, the beam emerging from the GaAs is passed through a polarizer oriented at 45° to the Y' and Z' axes. The intensity of the output beam is then

$$P_{\text{out}}(V) = P_0\left[1 + \sin\left(\frac{2\pi}{\lambda_0} n_0^3 r_{41} V\right)\right]$$

$$= P_o\left[1 + \sin\left(\frac{\pi V}{V_\pi}\right)\right] \tag{8}$$

where P_o is the output intensity with zero field in the substrate. V_π, called the half-wave-voltage, and given by

$$V_\pi = \frac{\lambda_0}{2n_0^3 r_{41}} \tag{9}$$

is the voltage required for 180° phase shift between the Y' and Z' polarizations. For GaAs, $V_\pi \cong 10$ kV at a wavelength of 1.064 μm for $n_0 = 3.6$, and $r_{41} \cong 1.4 \cdot 10^{-12}$ m/V [29]; the argument of the sine expression is thus small for typical voltages V on integrated circuits, and (8) can be approximated by

$$P_{\text{out}} \cong P_o\left[1 + \frac{\pi V}{V_\pi}\right]. \tag{10}$$

For substrate voltages to several hundred volts, the output beam intensity is nearly linear and in direct proportion to the voltage across the substrate. The intensity of the output beam, detected by a photodiode, is thus a measure of the voltage across the substrate of the IC.

B. Probing Geometries in GaAs IC's

The transmission modulator of Fig. 7 requires separate lenses for focusing and collecting the probe beam, precisely aligned on opposite sides of the wafer for IC measurements. Also, high-density interconnections on the circuit side of digital IC's and backside metallization on many microwave IC's would obstruct the beam passage through the wafer. Reflection-type probing geometries as shown in Fig. 8 provide better access to IC's, using a single lens for focusing and using the IC metallization for reflection. The frontside geometry is suitable for probing microstrip transmission lines of MMIC's. The backside geometry permits very tight focusing of the probing beam to a diameter limited by the numerical aperture of the focusing lens, and provides a probe beam modulation sensitive to the probed conductor's voltage but independent of nearby signal conductors for typical IC layout [30], a necessity for testing high-density IC's.

For microstrip transmission lines typically used in MMIC's, the fields extend laterally from the conductor roughly a distance equal the substrate thickness; the probe beam is focused from the top of the substrate through the fringing fields of the conductor to a beam spot size diameter approximately one-tenth of the substrate thickness so that it overlaps well with the fringing fields. Other MMIC's use planar transmission lines such as coplanar waveguide (CPW) for microwave interconnects. MSI/LSI circuits typically use thin metal lines (3–10 μm); the electric field distribution around the conductors is a strong function of their layout. For these types of interconnects and for planar transmission lines, the extent of the fields into the substrate is on the order of the distance between signal conductors and grounds. Typical IC substrate thickness (400–500 μm) is much greater than conductor spacings; the electric fields lie near the substrate surface, and the back of the substrate is nearly at an equipotential with respect to individual conductors on the IC surface. The optical probe, focused through the back of the substrate to a spot diameter less than or equal to the conductor width, is modulated by the voltage on the conductor nearly independent of signals from nearby conductors (see Section IV-B on digital circuits and Figs. 28 and 29 for examples of probing closely spaced IC conductors).

In both cases the optical probe is reflected from metalization on the IC. The signal is proportional to the amount of light reflected, and if the reflectivity of the metalization varies, ths signal strength also varies. The signal can be normalized to the amount of reflect light, but metalization

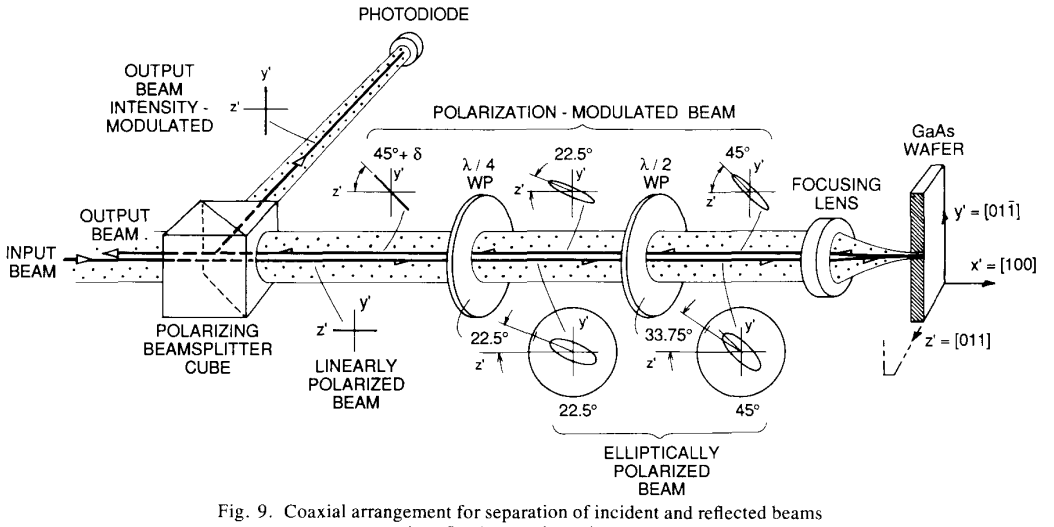

Fig. 9. Coaxial arrangement for separation of incident and reflected beams in reflection-mode probing.

such as ohmic contacts, which may be very rough, will cause poor signal sensitivity if a large fraction of the probe beam is scattered. Because integrated circuits are patterned by optical lithography, the wafer top surface has good optical quality. For backside probing the back of the wafer must be polished to allow passage of the probe beam with negligible scattering. For frontside probing the ground plane should be sufficiently reflective to provide a good return beam—most MMIC's we have encountered have shown adequate ground-plane reflectivity.

In reflection-mode probing, the incident and reflected beams, centered on the microscope lens for optimum focusing, can be separated by manipulation of their polarizations (Fig. 9). The advantages of this arrangement for IC probing are ease-of-alignment, on-axis focusing for diffraction-limited spot size, and efficient use of the optical signal (in contrast to using a beamsplitter to separate the incident and return beams, which attenuates half the optical power on each pass). The polarization states of this arrangement may be analyzed by Jones calculus, and are qualitatively described as follows. A linearly polarized probe beam from the polarizing beamsplitter passes through a quarter-waveplate, oriented at 22.5° to the axis of beamsplitter, producing an elliptical polarization. A half-waveplate oriented at 33.75° then rotates the elliptical polarization an additional 22.5° to align its major axis at 45° to the [011] direction of the GaAs substrate (i.e., oriented at 45° to the substrate cleave planes). The on-axis probe beam is focused by a microscope objective next to a conductor (frontside probing) or on the conductor (backside probing). The reflected beam passes back through the lens and the waveplates, producing a linear polarization at 45° to the axes of the polarizing beamsplitter, and the polarization component at 90° orientation is directed by the beamsplitter onto a photodiode. The probed conductor voltage changes the polarization of the return beam through the electrooptic effect by changing the *angle* of the linearly polarized light prior to the polarizer, and thus the intensity incident upon the photodiode. The resulting intensity varies as in (10) where V_π is now

$$V_\pi = \frac{\lambda_0}{4n_0^3 r_{41}} \cong 5 \text{ kV} \tag{11}$$

giving twice the sensitivity for the reflection-mode cases. The on-axis return beam may be separated from the incident beam with a Faraday isolator. The signal from this beam is out-of-phase with the first beam allowing for differential detection to further improve signal sensitivity.

C. Electrooptic Sampling

The longitudinal reflection-mode geometries provide intensity modulation proportional to voltage for IC probing. With a continuous optical probe beam, the ouput intensity incident upon the photodiode will be a large steady-state intensity P_0 plus a small intensity change following the voltage of the probed conductor; microwave-frequency or picosecond-risetime signals on the probed conductor will result in microwave-frequency or picosecond-risetime modulation of the probe beam. Detection of this modulation would require a photodiode/receiver system with bandwidth comparable to that of the detected signal. With commercial sampling oscilloscopes limited to ≈ 14 GHz and infrared photodiodes limited to ≈ 20 GHz, the probing system's bandwidth would be insufficient for many high-speed and microwave GaAs circuits. In addition, the small modulation provided by the electrooptic effect would result in extremely poor signal-to-noise ratio using direct detection at microwave bandwidths, and thus very poor instrument sensitivity.

Mode-locked laser systems in conjunction with optical pulse compressors can generate extremely short optical pulses. At visible wavelengths, pulses as short as 6 fs [31], [32] have been generated, while at the infrared wavelengths where GaAs is transparent, pulses as short as 33 fs have been generated [33], [34]. Sampling techniques

using a pulsed optical probe can achieve a time resolution set by the optical pulse duration and the circuit-probe interaction time, permitting instrument bandwidths exeeding 100 GHz. We describe repetitive sampling in the time domain as *synchronous sampling*, where equivalent-time measurements of the voltage waveforms are made in a manner similar to the operation of a sampling oscilloscope, and in the frequency domain as *harmonic mixing*, where the electrooptic sampler measures the amplitude and phase of sinusoidal voltages on probed conductors, similar to a microwave network analyzer.

In synchronous or equivalent-time sampling, an optical probe pulse with a repetition rate f_0 (set by the laser) samples a repetitive voltage waveform. If the waveform repeats at *exactly* $N*f_0$, an integer multiple of the probe repetition rate, an optical pulse interacts with the waveform every Nth period at a fixed point within its cycle. Over many repetitions, the pulses sample the voltage waveform at the same time within the cycle, undergoing an equal modulation of each pulse's intensity. The resulting change in the average intensity of the probe beam, proportional to the signal, is detected by a photodiode receiver whose bandwidth is much less than the optical pulse repetition frequency. To detect the entire time waveform, the waveform frequency is increased by a small amount Δf (Fig. 10.) The probe pulses are then slowly delayed with respect to the waveform, sampling successively delayed points, so that the average intensity at the photodiode changes in proportion to the waveform, but *repeating* at a rate Δf. The receiver then averages (low-pass filters) the photocurrent over a period much longer than $1/f_0$, eliminating the individual pulses. The averaged photocurrent i_{out} is then continuous and varies with $V(t)$, but at the slow repetition rate Δf

$$i_{\text{out}}(t) = I_0\left[1 + \frac{\pi}{V_\pi} V\left(\frac{t\Delta f}{Nf_0 + \Delta f}\right)\right] \qquad (12)$$

where I_0 is the average photodiode current. Typically f_0 is ≈ 82 MHz, N varies from 1 to 500 for circuit drive frequencies to 40 GHz, and Δf is 10 to 100 Hz. In contrast to pump/probe sampling, which has one probe pulse for every pump signal, the signal repeats N times between probe pulses in equivalent-time sampling. Because the pulse repetition rate is harmonically related to the signal repetition rate, Nyquist's sampling theorem (which states maximum recoverable signal bandwidth is half the sampling rate) does *not* apply in terms of setting the bandwidth of this measurement. Instead, the bandwidth is determined by the sampling pulsewidth, the relative jitter between sampling pulses, and the interaction time between the pulse and the signal. These factors are discussed in detail in Section III-B.

The frequency domain description of equivalent-time sampling is known as *harmonic mixing*. The time domain signal detected by the photodiode receiver, proportional to the product of the laser signal and the measured signal in the time domain, has a frequency spectrum determined

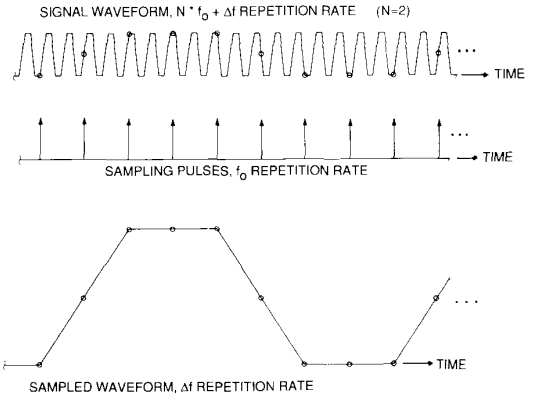

Fig. 10. Equivalent-time sampling. Typically, $f_0 \approx 82$ MHz, $0 \le N < 500$, and $\Delta f \approx 10$ Hz.

by the spectrum of the laser *convolved* with the spectrum of the measured signal [35]. In the frequency domain

$$\mathfrak{F}\{P_{\text{out}}(t)\} = \mathfrak{F}\{P(t)\} * \left[\delta(f) + \frac{\pi\mathfrak{F}\{V(t)\}}{V_\pi}\right] \qquad (13)$$

where $\mathfrak{F}$ is the Fourier transform operator, $P_{\text{out}}(t)$ is the intensity out of the polarizer, $P(t)$ is the laser intensity, $\delta(f)$ is the delta function, and $*$ represents the convolution operation. Fig. 11 shows a schematic representation of this convolution for a mode-locked laser spectrum and a single microwave frequency signal. Scaled replicas of the signal appear in the laser intensity spectrum as amplitude-modulation sidebands around each laser harmonic. The magnitude and phase of the signal is recovered from the baseband harmonic with a low-frequency photodiode and a synchronous detector.

III. System Performance

A. System Description

The sampling system, shown schematically in Fig. 12, can be grouped into three sections: the laser system for optical pulse generation, the microwave instrumentation for driving the IC under test, and the receiver system for signal processing and data acquisition. The laser system consists of a mode-locked Nd:YAG laser, a fiber-grating pulse compressor, and a timing stabilizer feedback system. The Nd:YAG laser produces 1.06 μm, 90 ps pulses at an 82 MHz rate with free-running pulse-to-pulse timing fluctuations of 4 ps rms, reduced to less than 300 fs rms by a phase-lock-loop feedback system [36], [37] which synchronizes and stabilizes the laser pulse timing with respect to the microwave synthesizer. The fiber-grating pulse compressor shortens the pulses to 1.5 ps FWHM (full width at half maximum) [38]–[40]. The beam passes through a polarizing beamsplitter and two waveplates to adjust its polarization, then is focused through the IC substrate with a microscope objective to a 3 μm spot on the probed conductor (backside probing) or a 10 μm spot on the ground plane beneath and adjacent to the probed conductor (frontside probing). The reflected light is analyzed

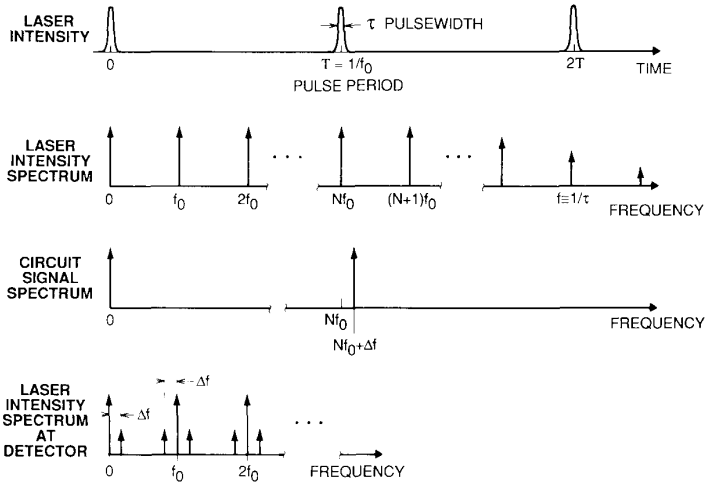

Fig. 11. Electrooptic harmonic mixing.

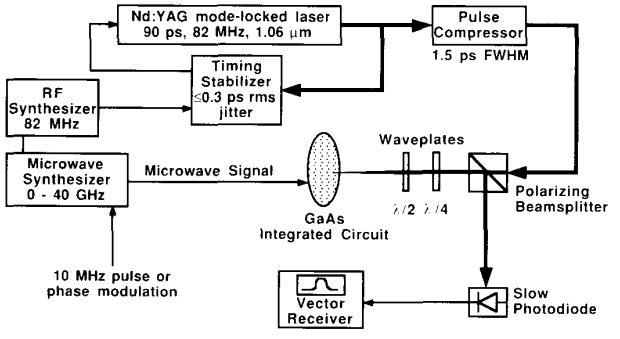

Fig. 12. System for direct electrooptic sampling.

by the polarizing beamsplitter and detected by a photodiode connected to a vector receiver.

To drive the IC, a microwave synthesizer generates either sinusoidal excitation for microwave circuits or the clock/data signals for digital circuits. For wafer-level testing of IC's the drive signal is delivered with a microwave probe station (Cascade Microtech Model 42, Figs. 13 and 14) modified to allow for backside electrooptic probing. The transmission line probes used with this test station allow for launching a signal on the IC with repeatable, low reflection connections in a 50 Ω environment to 50 GHz.

Signal processing is critical to achieve accurate, shot-noise limited measurements. Harmonic mixing is used for vector voltage measurements. The synthesizer is set to an exact multiple of the laser repetition rate plus a 1–10 MHz frequency offset, and the receiver is configured as a synchronous detector (i.e., an RF lock-in amplifier) to measure the magnitude and phase of the received signal at the frequency offset. Equivalent-time sampling is used to view time waveforms. The synthesizer is set to an exact multiple of the laser repetition rate (82 MHz), plus a small frequency offset Δf (1–100 Hz). Pulse modulation, phase modulation, or fast offset/averaging signal processing as described in Section III-C is required to suppress laser intensity noise. The resulting signal varies at the slow offset rate Δf in proportion to the detected signal.

Direct electrooptic sampling has also been demonstrated using a mode-locked or gain-switched In–GaAsP injection laser to generate sampling pulses of 10–20 ps pulsewidth [41]–[42]. This system uses two synthesizers, referenced to a master clock, to drive the laser and to supply a signal to the IC. The longer pulsewidths of the injection laser decrease the system's potential time resolution compared to the 1.5 ps pulsewidths generated using the Nd:YAG/pulse compressor, but the injection laser pulses have subpicosecond timing jitter and the laser is a very compact and stable optical source with a continuously tunable pulse repetition rate. This system has also been used to measure electrical signals in InP (indium phosphide) IC's [43].

B. Bandwidth

The system's bandwidth or time resolution is determined by the optical pulsewidth, the pulse-to-pulse timing jitter of the laser with respect to the microwave synthesizer driving the circuit, the interaction time of the probe pulse and the electrical signal, and the effective receiver response time. We assume Gaussian distributions for each term for simplicity. The overall time resolution is the root mean square sum of these values

$$\sigma_{\text{total}} = \sqrt{\sigma_{\text{PW}}^2 + \sigma_J^2 + \sigma_{\text{IT}}^2 + \sigma_{\text{REC}}^2} \qquad (14)$$

where σ_{PW} is the rms optical pulsewidth, σ_J is the rms pulse-to-pulse timing jitter, σ_{IT} is the rms interaction time of the pulse through substrate, and σ_{REC}^2 is the effective receiver impulse response time.

The relation between the time resolution and the frequency bandwidth for the optical pulse is given by

$$\sigma_{\text{FWHM}} = \frac{0.312}{f_{3\text{dB}}} \qquad (15)$$

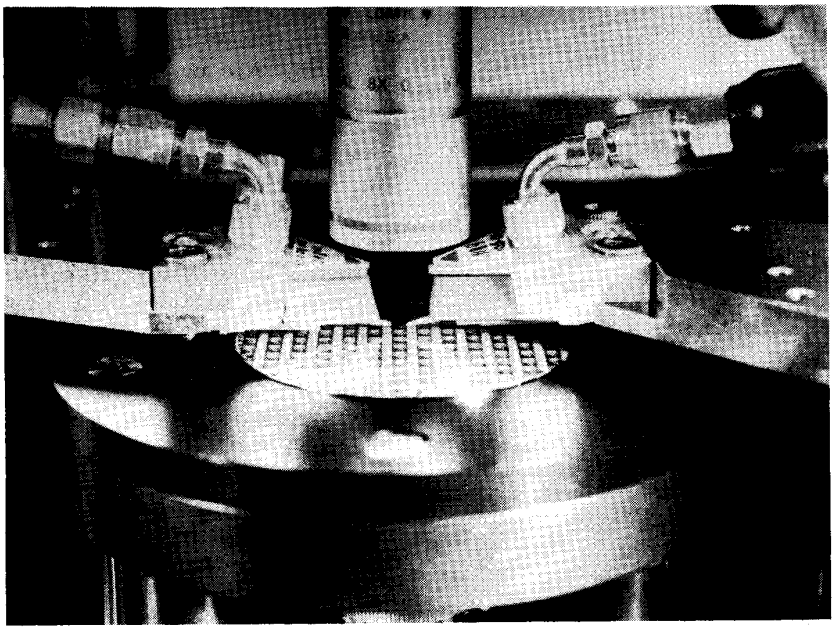

(a)

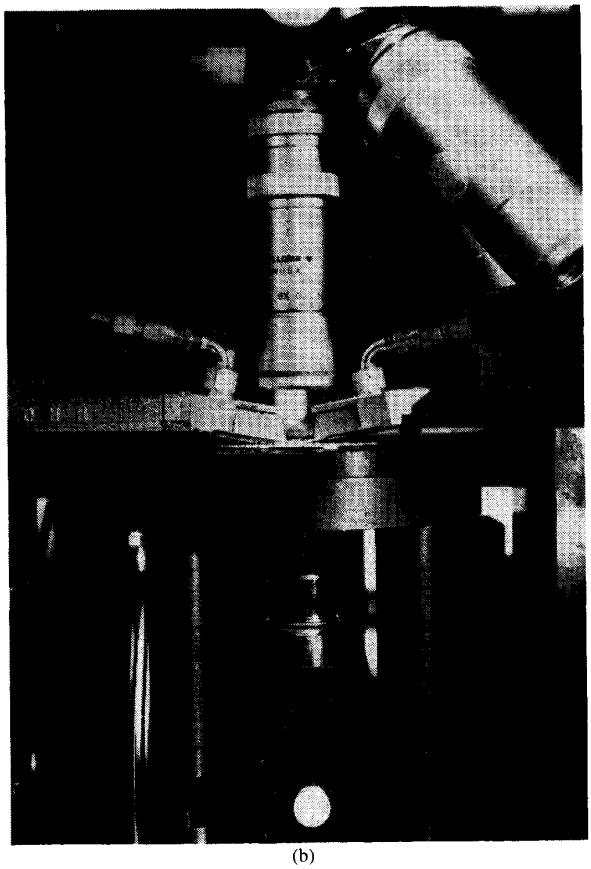

(b)

Fig. 13. Cascade microwave wafer probe station modified for electrooptic sampling. (a) Wafer, wafer stage, microwave wafer probes, and viewing objective. (b) View showing probe beam focusing objective below the wafer stage. The probe beam is focused on the IC through a hole or a sapphire window in the wafer stage.

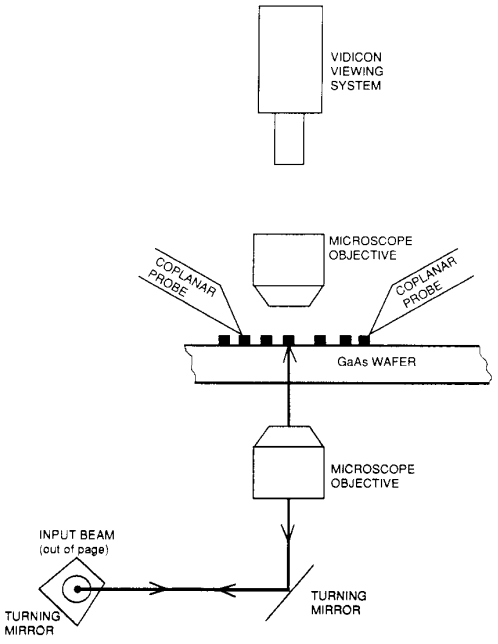

Fig. 14. Schematic diagram of the beam path through the Cascade probe station.

where for a Gaussian pulseshape $\sigma_{\text{FWHM}} = 2.35 * \sigma_{\text{rms}}$ is the full width at half maximum (optical pulsewidth is typically measured in terms of its FWHM, not its rms value), and $f_{3\,\text{dB}}$ is the half power frequency. This time-bandwidth product is reduced by a factor of $1/\sqrt{2}$ from the time-bandwidth product of 0.441 due to the square-law photodiode detector, i.e., the optical intensity of the pulse is converted to a voltage in the receiver with a resulting power spectrum related to the square of this voltage.

The 90 ps pulsewidth from the Nd:YAG laser results in a bandwidth of 3.5 GHz, clearly not suitable for high bandwidth circuit measurements. To reduce the pulsewidth, a fiber-grating pulse compressor is used [38]–[40]. This system, based on the Kerr effect or self-phase modulation in a single-mode optical fiber, generates a frequency chirp on the laser pulse as it propagates through the fiber. The light emerging from the fiber is red-shifted on its leading edge and blue-shifted on its trailing edge with the frequency varying across the pulse duration in proportion to the derivative of the intensity envelope. For a Gaussian intensity pulseshape (characteristic of some mode-locked lasers) the frequency chirp is nearly linear over the center of the pulse. These new frequency components are recombined into a compressed pulse by passing the light through a grating pair, where the time-of-flight delay is linearly proportional to the light's wavelength, thus acting as a dispersive delay line where the red-shifted leading frequency components are delayed with respect to the blue-shifting trailing frequencies. The wavelength-dependent delay is adjusted by the separation of the gratings to match the frequency chirp of the light, producing a compressed pulse.

A number of effects limit the amount of pulse compression available with this technique; stimulated Raman scattering limits the maximum optical power focused into the fiber core, and deviation from a linear frequency chirp on the pulse due to nonideal input pulseshapes can generate long pedestals on an otherwise short compressed pulse. Using a fiber length of 1 km in the pulse compressor, the group velocity dispersion enhances the region of linear frequency chirp [39], and the pulses from the mode-locked Nd:YAG laser are routinely compressed to 1.5 ps, a factor of 60:1. Using two-stage optical compression, pulses as short as 200 fs at 1.06 μm have been generated [34].

The compressed pulsewidth, as measured with an optical autocorrelator, deviates from the autocorrelation of an ideal Gaussian pulseshape as evidenced by slight "wings" or pedestals on the pulse due to nonideal frequency chirp on the pulse (Fig. 15). The group velocity dispersion of the relatively long 1 km fiber reduces the pulse pedestals compared to shorter fiber lengths [39]. A Gaussian pulse of 1.4 ps FWHM duration has spectral content extending past 200 GHz, while the spectral content of the compressed pulse deviates from an ideal Gaussian pulse, where the power spectral density is determined by numerically Fourier transforming the autocorrelation (Fig. 16) [35]. The wings on the compressed pulse may be further reduced by "spectral windowing" [44] to remove part of the nonlinear frequency chirp or polarization discrimination of the compressed pulse [45].

Timing jitter influences both bandwith and sensitivity; the impulse response of the sampling system is the convolution of the optical pulseshape with the probability distribution of its arrival time (neglecting optical transit time), while those Fourier components of the jitter lying within the detection bandwidth of the receiver introduce noise proportional to the time derivative of the measured waveform (Section III-C). Stabilization on the laser timing is thus imperative for low-noise measurements of microwave or picosecond signals. The timing fluctuations of the laser are suppressed by phase-locking the laser to a high-stability reference oscillator [36], [37]. Fig. 17 shows the block diagram of the feedback system. A photodiode monitors the 82 MHz laser pulse train, and the phase of its fundamental component is compared with that of the reference oscillator, generating a phase error signal. The 41 MHz signal required for driving the laser's acoustooptic (A-O) cell is generated by frequency division from the 82 MHz standard; its timing (phase) is adjusted with a voltage-controlled phase-shifter controlled by the amplified and frequency-compensated phase error signal. Given an error-free phase detector, the laser timing fluctuations are suppressed in proportion to the loop gain of the feedback system. Fig. 18 shows the measured phase noise of one harmonic of the laser with an HP 8662 low-phase noise synthesizer as the reference for the feedback system. From this measurement the time jitter is calculated [see Section III-C, (26)] to be less than 300 fs rms.

The interaction time of the optical pulse and electrical signal in the GaAs substrate comes from several factors; the response time of the electrooptic effect, the electrical transit time, and the optical transit time. The electrooptic

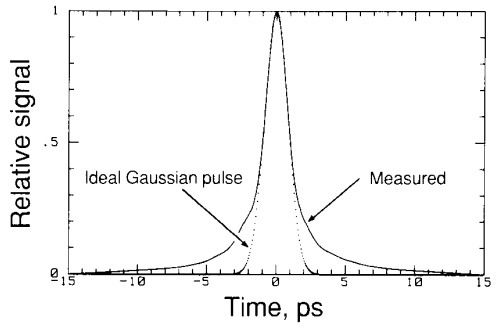

Fig. 15. Autocorrelation of the 1.4 ps FWHM compressed pulse (solid line) and the autocorrelation of an ideal Gaussian pulse (dashed line).

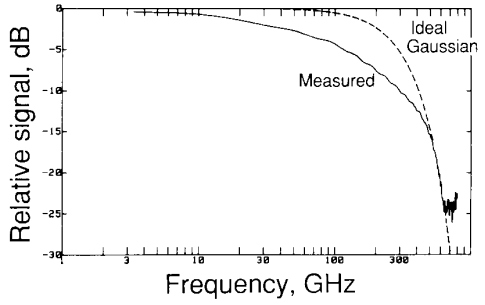

Fig. 16. Power spectral density of the compressed pulse (solid line) and a Gaussian pulse (dashed line). The power spectral density is the Fourier transform of the autocorrelation.

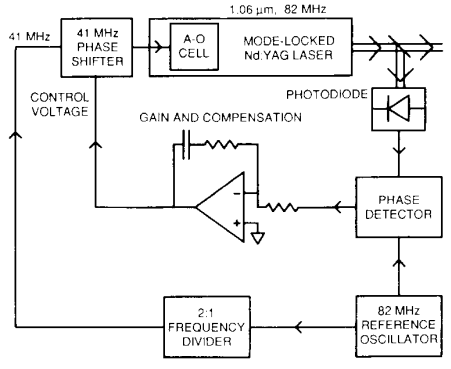

Fig. 17. Block diagram of the phase-lock-loop timing stabilizer feedback system.

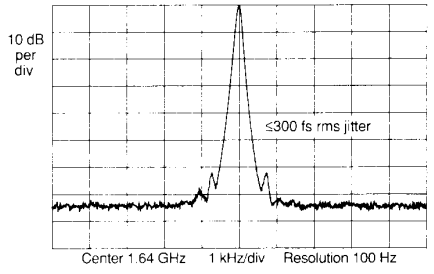

Fig. 18. Laser phase noise at the 20th harmonic of the pulse repetition rate, measured with a photodiode and a spectrum analyzer. The noise floor of this measurement is instrumentation limited, giving an upper

effect in GaAs arises primarily from its electronic polarizability and is intrinsically very fast (see Auston, this issue), with a response time on the order of 10 fs. The electrical transit time is the propagation time of the electrical signal as it traverses the spatial extent of the probe beam. For typical IC values this time is on the order of 60 fs [27]. The optical transit time is the propagation time of the optical pulse as it traverses the electric fields within the GaAs substrate. For frontside probing of microstrip lines, where the field is uniform though the substrate, the optical transit time is proportional to the substrate thickness. For backside probing of coplanar transmission lines or planar interconnections, the electric field is not uniform in the substrate and the characteristic depth of the electric fields is on the order of the conductor spacing; in this case the optical transit time is not a function of substrate thickness, but a function of the conductor spacing. Because the optical and microwave dielectric constants in GaAs are nearly equal, microwave transmission lines have a cutoff frequency for higher order modes roughly equal the inverse of the optical transit time. Well-designed microwave circuits operate at frequencies well below the multimode cutoff frequency. Only when measuring interconnects near or above the cutoff frequency (where dispersive characteristics are of interest) must the optical transit time be considered. For example, the optical transit time for a 125 μm thick substrate, typical of MMIC's operating at frequencies below 40 GHz, is 3 ps, corresponding to a 3 dB response rolloff of $>$ 100 GHz.

The effective receiver impulse risetime arises from the constraint put on the receiver bandwidth by the required system sensitivity. We assume for analysis the receiver has a Gaussian impulse response

$$h(t) = \frac{1}{\sqrt{2\pi}\sigma_t} \exp\left(\frac{-t^2}{2\sigma_t}\right) \tag{16}$$

where σ_t is the rms duration. Then, the receiver frequency response

$$H(f) = \exp\left(\frac{-f^2}{2B_{\text{acq}}}\right) \tag{17}$$

has an rms signal acquisition bandwidth $B_{\text{acq}} = 1/2\pi\sigma_t$. Because the sampled signal at frequency Nf_0 is translated to a lower frequency Δf at the receiver (12), the effective receiver impulse response for synchronous sampling is

$$\sigma_{\text{REC}} = \frac{\Delta f}{Nf_0}\sigma_t = \frac{\Delta f}{Nf_0 2\pi B_{\text{acq}}}. \tag{18}$$

Given a required time resolution σ_{total} from the electrooptic sampling system, the data acquisition rate of the sampler is then limited. For a fixed time resolution, larger receiver bandwidths B_{acq} (or shorter receiver time constants) permit faster waveform acquisition rates, but degrade the measurement sensitivity.

C. Sensitivity

If the measurement bandwidth provided by the electr[illegible] sampler is to be useful, the instrument must also

provide sufficient sensitivity to observe signal voltages typical of high-speed GaAs circuits. As in any system, sensitivity is determined by the signal to noise ratio; the instrument's sensitivity, or minimum detectable voltage, is the probed voltage which results in a measured signal equal to the measurement system's noise signal. Most noise sources have power spectral densities which are independent of frequency ("white" noise), resulting in a noise voltage proportional to the square root of the signal acquisition bandwidth B_{acq} and a minimum detectable voltage expressed in units of volts per root Hertz ($\text{V}/\sqrt{\text{Hz}}$). Smaller minimum detectable voltages permit more rapid measurement acquisition for fixed measurement accuracy. With appropriate system design and signal processing, the various sources of noise in the electrooptic sampler can be reduced or eliminated, permitting low-noise voltage measurements with fast data acquisition.

The fundamental limiting noise source in electrooptic sampling is the shot noise of the probe beam (observed as shot noise of the photodiode quiescent current.) The signal generated by the photodiode (dropping the constant term I_0) from (12) is

$$i_{\text{out}}(t) = \frac{I_0 \pi}{V_\pi} V\left(\frac{t\Delta f}{Nf_0 + \Delta f}\right) + i_{\text{SN}}. \tag{20}$$

The shot noise i_{SN} associated with the dc component of the photodiode current has a variance given by

$$\overline{i_{\text{SN}}^2} = 2qI_0 B_{eq} \tag{21}$$

where q is the electron charge, the horizontal bar denotes the statistical expectation, and

$$B_{eq} = \sqrt{\pi/2}\, B_{\text{acq}} \tag{22}$$

is the receiver's equivalent noise bandwidth. Setting the signal current $I_0 \pi V_{\text{min}}/V_\pi$ equal to the shot noise current, and normalizing to $B_{\text{eq}} = 1$ Hz acquisition bandwidth, the minimum detectable voltage is

$$V_{\text{min}} = \frac{V_\pi}{\pi}\sqrt{\frac{2q}{I_0}}\,\frac{\text{Volts}}{\sqrt{\text{Hz}}}. \tag{23}$$

For the reflection-mode probing geometries, $V_\pi \approx 5$ kV, while the average photocurrent I_0 is typically 1 mA. Then, the minimum detectable voltage is

$$V_{\text{min}} = 30\ \mu\text{V}/\sqrt{\text{Hz}} \tag{24}$$

Typically, $V_{\text{min}} \approx 70\ \mu\text{V}/\sqrt{\text{Hz}}$ is observed experimentally (at 1 mA average photocurrent) due to ≈ 10 dB of residual noise from the system (dominated by excess amplitude noise from the pulse compressor); this sensitivity is sufficient to acquire measurements at scan rates of 10–100 Hz with a noise floor of a few millivolts. The actual measurement system has a number of additional noise sources to contend with to achieve $70\ \mu\text{V}/\sqrt{\text{Hz}}$ sensitivity. These include timing jitter of the laser (phase noise), intensity noise of the probe beam from low frequency laser fluctuations and from the pulse compressor, and receiver noise.

Low-frequency fluctuations in the mode-locked laser introduce noise into the received photocurrent. Fluctuations in the mode-locked Nd:YAG laser include variations in both pulse intensity and pulse timing. The laser produces a train of pulses approximated by

$$P(t) = \frac{P_0}{f_0}\left[1 + N(t)\right] \sum_{m=-\infty}^{+\infty} \delta\left[t - m/f_0 - J(t)\right] \tag{25}$$

where $N(t)$ is the normalized pulse intensity fluctuation and $J(t)$ is the pulse timing fluctuation. The laser intensity then has a power spectral density $S_p(f)$ approximated to second order in $mf_0\sigma_J$ by

$$\begin{aligned} S_p(f) \approx P_0^2 \sum_{m=-\infty}^{+\infty} & \cdot \left\{\left[1 - (2\pi m f_0 \sigma_J)^2\right]\delta(f - mf_0)\right. \\ & + \left[1 - (2\pi m f_0 \sigma_J)^2\right] S_N(f - mf_0) \\ & \left. + (2\pi m f_0)^2\, S_J(f - mf_0)\right\} \end{aligned} \tag{26}$$

where $S_N(f)$ is the power spectral density of $N(t)$ and $S_J(f)$ is the power spectral density of $J(t)$. The spectrum of the laser intensity is a series of discrete spectral lines at multiples of f_0, plus spectra resulting from the timing and amplitude fluctuations, referred to as amplitude-noise sidebands $[S_N(f - mf_0)]$ and phase-noise sidebands $[(2\pi m f_0)^2\, S_J(f - mf_0)]$. By monitoring the laser intensity with a spectrum analyzer and measuring the relative powers of the laser harmonic and its noise sidebands as a function of the order of the harmonic, the spectral densities of $N(t)$ and $J(t)$ are measured.

With these amplitude and timing fluctuations, the received photocurrent $i_{\text{out}}(t)$ is

$$\begin{aligned} i_{\text{out}}(t) \approx I_0 + \frac{I_0 \pi}{V_\pi} V\left(\frac{t\Delta f}{Nf_0 + \Delta f}\right) + i_{\text{laser},0} \\ + i_{\text{laser},1} + i_{\text{phase}} \end{aligned} \tag{27}$$

where

$$i_{\text{laser},0} = I_0 N(t) \tag{28}$$

is the zero-order (background) received noise current due to laser intensity fluctuations,

$$i_{\text{laser},1} = N(t)\,\frac{I_0 \pi}{V_\pi} V\left(\frac{t\Delta f}{Nf_0 + \Delta f}\right) \tag{29}$$

is a received noise current arising from the product of the laser intensity fluctuations and the signal voltage, and

$$i_{\text{phase}} = \frac{I_0 \pi}{V_\pi} J(t)\, V'\left(\frac{t\Delta f}{Nf_0 + \Delta f}\right) \tag{30}$$

is the noise arising from the laser timing fluctuations, where $V'(t)$ is the time derivative of $V(t)$. We have assumed that $\Delta f \ll Nf_0$, and have omitted terms in $N(t) \cdot J(t)$, as these are negligible.

The spectral density $S_N(f)$ of the laser intensity noise $N(t)$ is shown in Fig. 19. At frequencies below $\approx$ 1 kHz, the laser intensity noise is approximately 70 dB greater than the shot noise of a 0.5 mA receiver photocurrent. At higher frequencies the noise power decreases, reaching an asymptote 5–15 dB above the shot noise level at frequencies greater than $\approx$ 100 kHz. The excess noise at frequencies above 100 kHz arises from Raman scattering and polarization noise in the optical pulse compressor. If the sampled signal were detected at a low frequency, the zero-order laser intensity noise $i_{\text{laser},0}$ would contribute a $10^3:1$ degradation to the minimum detectable voltage. To suppress the zero-order laser intensity noise, the excitation to the circuit under test is modified so that the received photocurrent $i_{\text{out}}(t)$ has a spectral component, with amplitude proportional to the proportional to the probed voltage, at a frequency above the 100 kHz $1/f$ noise corner frequency. One method is pulse modulation (chopping) of the drive signal. The received photocurrent then has a spectral component at the chopping rate whose amplitude varies in proportion to the sampled point on the signal waveform. The chopping frequency is set from 1–10 MHz, well above the $1/f$ noise corner frequency, to achieve near-shot-noise limited detection.

Driving digital IC's requires modification of the pulse modulation scheme, since most digital circuits require *continuous* drive signals for their clocks. One alternative is phase modulation of the drive signal, corresponding to controlled jitter in time, at the chopping frequency. The received photocurrent then has a component at the chopping frequency whose amplitude is proportional to the time derivative of the sampled signal, and is recovered by integration [46]. The drawbacks to this technique are circuit sensitivity to clock jitter (usually negligible) and a reduction in the signal-to-noise ratio (due to the differentiation). A second signal recovery scheme, termed fast offset and averaging, relies on increasing the frequency offset Δf to a rate above the low-frequency laser noise, 100–200 KHz. The signal is recovered by high-pass filtering to remove the low-frequency laser noise, then by signal averaging at the offset rate Δf. If the received signal is averaged at the scan rate, the sensitivity using fast averaging is the same as for simple synchronous sampling with the same measurement acquisition time. Commercial digitizing oscilloscopes have limited averaging rates; at scan rates of 100–200 kHz, most instruments can average a maximum of only 100–200 scans/s, corresponding to a signal-to-noise reduction of 30 dB from averaging at the fast scan rate. Even so, we have demonstrated the feasibility of this technique using a commercially digitizing oscilloscope, and the signal-to-noise reduction, compensated for by the increased measurement acquisition time, is justified for testing IC's that are sensitive to signal chopping.

The two remaining noise terms arising from laser low-frequency fluctuations, $i_{\text{laser},1}$ and i_{phase}, are not suppressed by signal chopping or signal phase modulation. Because these noise terms arise from the products $N(t)$ $V(\alpha t)$ and $J(t)$ $V'(\alpha t)$, their power spectra are proportional to the convolutions $S_N(f) * S_V(f/\alpha)$ and $S_J(f) * f^2 S_V(f/\alpha)$, respectively, where $S_V(f)$ is the power spectrum of $V(t)$. Pulse-modulation or phase-modulation of $V(t)$ at a frequency f_{mod} results in a received photocurrent having spectral components at f_{mod} arising from both $V(t)$ and from the multiplicative laser amplitude noise $i_{\text{laser},1}$ and the received phase noise i_{phase}. Instead, these noise terms must be suppressed by laser stabilization. The laser timing stabilizer reduces $S_J(f)$ by 20–25 dB at frequencies lying within typical receiver bandwidths B_{acq} of 10 Hz–1 kHz. Fig. 20 shows the resulting suppression of received phase noise on a 20 GHz sampled signal. The multplicative amplitude noise $i_{\text{laser},1}$ can be suppressed by feedback stabilization of the laser intensity [47]. As the multiplicative amplitude noise scales with the signal voltage $V(t)$, without laser amplitude stabilization it is a significant source of measurement error in the electrooptic sampling system for signal voltages larger than $\approx$ 1 V.

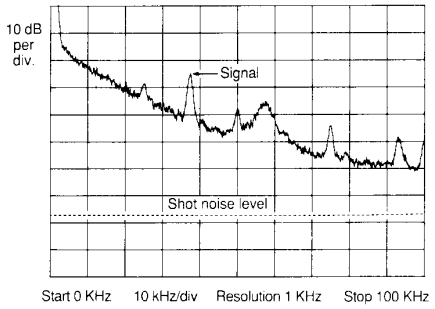

Fig. 19. Spectrum of the laser intensity noise, measured with a photodiode and spectrum analyzer. At low frequencies the intensity noise is approximately 70 dB above shot noise (for a 0.5 mA photocurrent).

Additional noise arises from the receiver, which has an equivalent input noise current

$$\overline{i^2_{\text{receiver}}} = \frac{4kTB_{eq}}{R_L} + \overline{i^2_{\text{amp}}} + \frac{1}{R_L^2}\overline{v^2_{\text{amp}}} \tag{31}$$

where k is Boltzmann's constant, T is the absolute temperature, and R_L is the photodiode load resistor. The first term is the Johnson or thermal noise of the load resistor, and i^2_{amp} and v^2_{amp} are the equivalent input noise current and equivalent input noise voltage of the amplifier following the photodiode. Receiver noise is reduced to a level below the shot noise limit by appropriate receiver design; R_L is made large in comparison with $2kT/qI_0$ so that Johnson noise is well below shot noise and the photodiode amplifier is selected for low input noise.

The pulse compressor introduces excess amplitude noise due to stimulated Raman scattering (SRS) and temperature-induced polarization drift in the nonpolarization-preserving fiber [48]. We observe the broadband background amplitude noise increase dramatically (20–40 dB) above the shot noise limit as the input power to the fiber approaches the Raman threshold. A periodic structure to the noise spectrum (Fig. 21) corresponds to the free-spectral

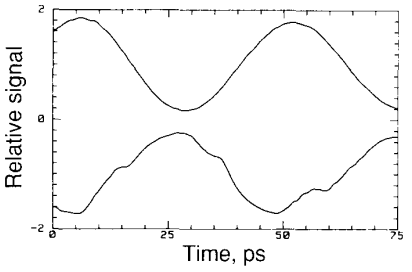

Fig. 20. 20 GHz sampled signal with (upper trace) and without (lower trace) timing stabilizer.

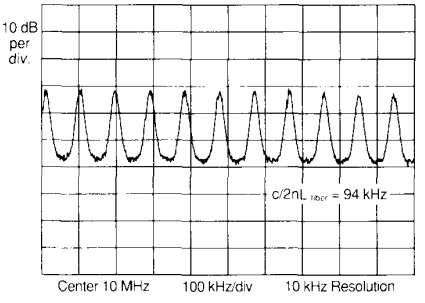

Fig. 21. Periodic noise spectrum indicative of a parasitic fiber-Raman laser for the pulse compressor operated near the stimulated Raman threshold.

range of the 1 km fiber. We attribute this effect to a parasitic synchronously pumped fiber-Raman laser formed by the 4 percent Fresnel reflection at each fiber end facet and the high gain of the 1.06 μm pumped SRS [49], [50]. Self-phase modulation (SPM) occurs over the entire length of the fiber while the interaction length for SRS is set by the dispersion-induced walkoff between the input and Stokes-shifted wavelengths, approximately 60 m. This dispersion also causes the 1.06 μm pump and the 1.12 μm Raman pulse to separate by 1.8 ns over the length of the 1 km fiber. If the weakly-reflected Raman pulse is synchronized to within 1.8 ns of a pump pulse it is further amplified after its first round trip through the fiber. With this condition the Raman threshold with the 1 km fiber is 400 mW average power from the fiber output. Trimming the fiber length a few inches defeats this synchronism and increases the Raman threshold to 700 mW. We routinely obtain 60X compression ratios at power levels (350 mW average power from the fiber output) well below the Raman threshold.

In addition to SRS the fiber generates broadband polarization noise, possibly arising from guided acoustic wave Brillioun scattering [51] or intensity-induced polarization fluctuations [45]. The polarization noise is converted to amplitude noise after passing through the grating pair in the compressor. Adjusting the polarization from the fiber to maximize transmission through the grating path results in second-order intensity variations due to polarization fluctuations, reducing this excess noise to a level approaching the shot noise limit (Fig. 22). However, the pulse compressor with the relatively long 1 km fiber typically contributes 5 to 15 dB of excess amplitude noise. To suppress polarization drift, the nonpolarization-preserving fiber is placed in a temperature-stabilized environment.

D. Spatial Resolution

The spatial resolution of the probe is set by diffraction-limited focusing of the 1.06 μm wavelength beam. The minimum achievable spot diameter (full width half maximum) for diffraction limited optics is

$$d_0 \cong \frac{\lambda\sqrt{1 - \mathrm{NA}^2}}{2\mathrm{NA}} \tag{32}$$

where λ is the optical wavelength and NA is the numerical aperture of the focusing lens. With a high NA, lens spot sizes approaching the optical wavelength are possible. Standard microscope objectives (focal length of 8 mm and NA of 0.4, for example) routinely achieve spot sizes of 3 μm, suitable for probing most IC interconnects but not for probing very small features such as sub-micron gate lines.

E. Linearity

Because typical circuit voltages are small compared to the half-wave voltage V_π, the probe beam intensity modulation is small and very nearly linear with respect to the probed voltage. An analysis of the linearity and dynamic range of the probe due to the sinusoidal dependence of the probe intensity with respect to signal voltage [27] shows the probe is linear to within 1 percent for signal voltages ≤ 200 volts with the system set at the quarter-wave bias (the linear region of the sinusoidal transmission) as in (8).

F. Invasiveness

One important feature of optical probing of IC's is the noncontact, nondestructive nature of the technique. Compared to conventional electrical probes, the optical probe makes no mechanical contact to the IC, avoiding physical damage to the circuit, does not require the test point to drive a 50 Ω load impedance, and has no parasitic impedances. The lack of parasitic impedances is an important characteristic for measurement frequencies in the upper microwave and millimeter-wave region, where even the small parasitic impedances of well-designed electrical probes become significant. The optical probe can perturb the circuit either by photogenerating carriers, which then change the substrate conductivity and generate photorefractive or photovoltaic potentials, or by the inverse electrooptic effect or optical rectification. Direct band-to-band absorption of the probe is avoided because the photon energy of the 1.06 μm optical probe, 1.17 eV, is well below the bandgap energy, 1.42 eV, of GaAs. However, the presence of impurities in the GaAs results in deep levels, i.e., the presence of allowed electron states at energies near mid-bandgap. The deep levels, primarily the EL2 level, absorbed some of the 1.06 μm light in the GaAs and generate free carriers. Absorption can also occur if the probe beam is too intense. With tight beam focusing and short pulse duration, probe beams of average inten-

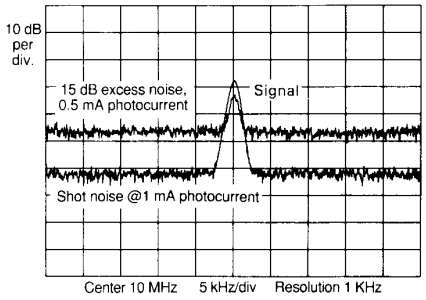

Fig. 22. Excess amplitude noise due to misadjustment of the polarization from the output of the pulse compressor fiber.

sities approaching 100 mW have peak pulse intensities sufficient for two-photon band-to-band absorption.

On circuits, we observe changes of approximately 0.1 dB in the forward gain (S_{21}) of microwave distributed amplifiers with an intense 125 mW probe beam at 1.06 μm wavelength. Focusing *directly* within the active FET channel causes significant changes in drain current. However, the probe is not focused within the device for circuit measurements, but on the adjacent metal interconnects. For testing digital circuits probe beam intensities are kept below ~50 mW typically. Probe beam intensities can be reduced by a factor of ten, reducing the photogenerated carrier concentration by a similar factor, without severe degradation of the system sensitivity (23). Residual invasiveness of the probe can also be reduced by increasing the probing wavelength from 1.06 to 1.3 μm, where the absorption due to the EL2 deep level is reduced by a factor of 5 [52], [53].

IV. Circuit Measurements

A. Realistic Circuit Testing Conditions

Optical probing, providing access to the high-impedance internal nodes of IC's with picosecond time resolution and micron spatial resolution, permits direct measurements of the performance of state-of-the-art microwave and digital GaAs circuits. To permit meaningful evaluations of a circuit's performance and to provide meaningful comparisons between competing circuit technologies, these measurements must be made under realistic circuit operating conditions. The propagation delay of switching devices in simple test circuits, measured by either electrooptic sampling or by conventional methods, is used to project the maximum clock frequency of these devices used in digital systems. Unless the test circuit provides representative switching voltages, interface impedances, and fanouts, the measured delays will not correlate well with the maximum clock frequency of circuits such as shift registers, binary multipliers, and memory. For example, the response of a transistor driven by a low-impedance photoconductor and loaded by a low-impedance, 50 Ω transmission line is in general much faster than the response of a logic gate driven by the normal output impedance of a driving gate and loaded by the normal input capacitances of cascaded gates. If the test circuit is constructed in hybrid form with wire bonds between the tested device and the transmission lines, the interconnect parasitics may dominate the circuit response.

Ring oscillators and inverter strings, the simplest digital test structures, are often used as benchmarks of circuit speed. These circuits load the gates with unity fan-out and tend to give optimistically small delay measurements. Ring oscillators often operate small-signal, without full logic-level swings, while inverter strings operate with full logic-level swings. Master-slave flip-flops, connected as binary frequency dividers, operate with logic signal levels and with each gate loaded by a fan-out of two, and serve as better performance indicators.

For microwave/analog circuits such as distributed amplifiers, appropriate test signals are swept-frequency sinusoids for small-signal transfer function measurements, or single-frequency signals set to larger amplitudes for large-signal and saturation measurements. Signal source and terminations should have 50 Ω impedances to eliminate source and load reflections.

B. Digital Circuit Measurements

Ring oscillators provide a measure of a gate delay from the rate of free-running signal propagating around an odd-numbered ring of inverters, i.e., the repetition period corresponds to product of the average gate delay and the number of gates. These free-running circuits are not readily clocked with an external signal, making synchronization to the probe pulses for electrooptic sampling difficult. Inverter chains, however, consisting of series of cascaded inverting logic gates, must be clocked with an external signal, permitting the synchronization of probe pulses for electrooptic measurements and assuring full logic-level switching of the gates. Typically, average gate delays are measured with sampling oscilloscopes; the propagation delay of the entire chain is measured and divided by the number of inverters to obtain the average delay of an individual inverter. For electrooptic testing the input inverter is switched with a microwave synthesizer, generating a square wave that ripples through the test structure. The first several inverters condition the input signal, sharpening the switching transients until the signal risetimes and falltimes reach a steady-state value. The optical probe is then positioned from node-to-node, measuring directly the propagating delays and signal risetimes at gate input and output nodes internal to the gate.

Fig. 23 shows a gate delay measurement on an inverter chain implemented in 1 μm gate-length buffered-FET logic MESFETS, with Fig. 24 showing an SEM picture of one inverter. The delay between curves A and B of Fig. 23 is the propagation delay of the inverting common-source stage, 60 ps, while the delay between curves B and C is the delay of the source-follower buffer and diode level-shifter, 15 ps. The inverter chain from Lawrence Livermore National Labs [54] consisted of 20 gates each with a fan-in and fan-out of unity.

The timing of inverter chains has also been examined by Zhang *et al.* [55], optically triggering an inverter in

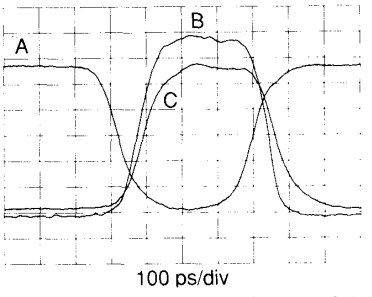

Fig. 23. (a) Voltage waveforms at the input (b) source-follower gate, and (c) output of GaAs buffered-FET-logic inverter gate [46], [54].

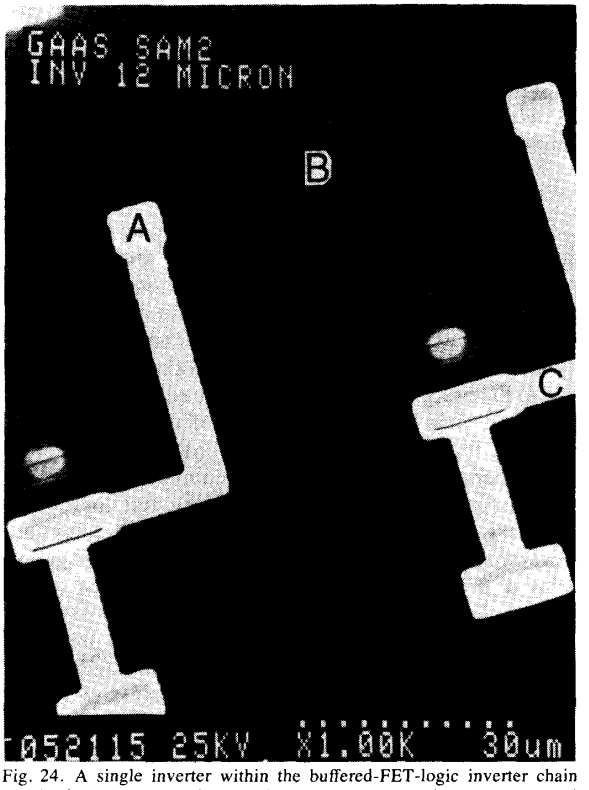

Fig. 24. A single inverter within the buffered-FET-logic inverter chain [54]. Photo courtesy S. Swierkowski, Lawrence Livermore National Labs.

the chain and using electrooptic sampling to measure the circuit response and gate propagation delays in a pump/probe configuration. A frequency-doubled portion of the probe beam (at $\lambda = 532$ nm) focused on the gate region of a FET generates carriers, turning on the FET and generating a switching transient that propagates down the test structure. The probe beam, positioned at a node after the switched gate, is successively delayed with respect to the switching pulse to map the transient waveform. This technique offers an all-optical approach, avoiding microwave connection to the IC, which is suitable for testing of simple IC test structures. However, optical triggering is an impractical method for generating the multiple clock and data signals required to drive large scale IC's.

A higher-level test circuit for IC performance is the static frequency divider, consisting of two flip-flops in a master-slave divide-by-two arrangement [4]. The maximum clock frequency of the divider, set by the propagation delays through the master-slave feedback path, provide an indirect measure of the devices' speed. Testing this circuit is normally accomplished by increasing the clock rate of the divider until its divide-by-two output fails.

The schematic of such a frequency divider is shown in Fig. 25. The circuit, from Hughes Research Laboratories (see Fig. 26), uses 0.2-μm E-beam written gates, molecular-beam epitaxy grown channels, air-bridge interconnects, and optimized feedback to achieve high frequency clock rates. The dividers were implemented in two circuit families, buffered-FET logic (BFL) and capacitively enhanced logic (CEL). Conventional testing, using transmission line probes to drive the circuit and monitor its output on a spectrum analyzer indicated correct circuit operation to 18 GHz. However, the spectrum analyzer gives inconclusive evidence of correct divider operation, since it measures only the output frequency and not the time waveforms. By direct waveform measurements using electrooptic sampling, correct divide-by-two operation was verified, gate propagation delays of 20–30 ps were measured and correlated to maximum clock frequencies (Fig. 27), and the internal delays through the inverting and source-follower stages of individual BFL stages of individual BFL gates were identified [56]. Note that while the scaled 0.2 μm gate-length FET's had significantly shorter delay through the inverting stage, the delay through the buffer stage was comparable to the 1 μm BFL from LLNL. These data suggest the speed limitation through the buffer stage is no longer *transistor* limited but limited by the resistance-capacitance time constant of the level-shifting diode resistance and the input capacitance of the cascaded gates.

The spatial resolution of the electrooptic sampler permits probing of MSI GaAs digital IC's to determine signal risetimes and relative timing. Fig. 28 shows serial output waveform probed on a 2 μm conductor internal to the output buffer in a 2.7 GHz 8 bit multiplexer/demultiplexer from TriQuint Semiconductor [57] and Fig. 29 shows the 8-phase clock waveforms probed on 3 μm metal interconnects spaced by 6 μm. Similar measurements have recently been made on gigahertz logic flip-flops and counters [58].

C. Microwave Circuit Measurements

At microwave and millimeter-wave frequencies, where conductor lengths and circuit element sizes often become large with respect to the electrical wavelength, direct measurements of conductor voltages and currents are difficult, particularly with conventional electrical test instrumentation. Directional couplers and directional bridges separate the forward and reverse waves on a transmission

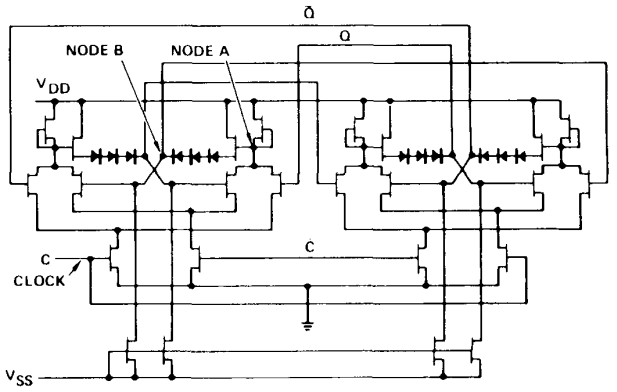

Fig. 25. Schematic diagram of a static frequency divider using buffer-FET logic. The labeled points refer to the electrooptically measured data in Fig. 27.

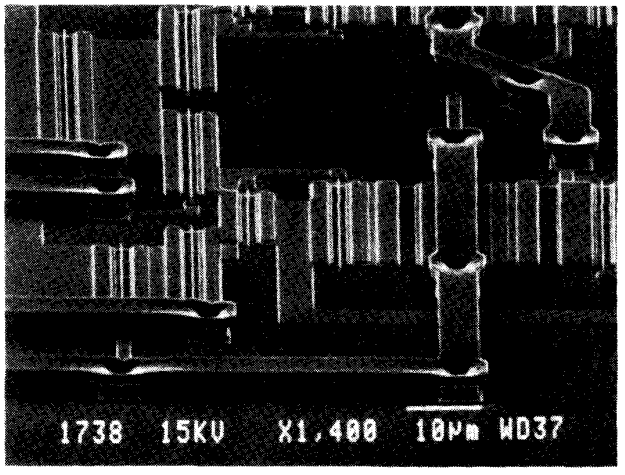

Fig. 26. Scanning-electron microscope picture of a section of an 18 GHz static frequency divider [4], courtesy of J. F. Jensen, Hughes Research Laboratories. The circuit uses 0.2 μm e-beam written gates, molecular-beam epitaxy-grown channels, air-bridge lines to reduce interconnect capacitance, and optimized feedback to achieve high-frequency clock rates.

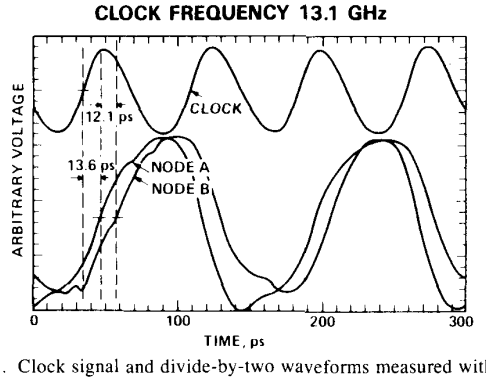

Fig. 27. Clock signal and divide-by-two waveforms measured with direct electrooptic sampling. The test points are indicated in Fig. 25.

line; standard microwave test instruments use these to measure the incident and reflected waves at the ports of a microwave device or network. The relationship between these waves is known as the *scattering parameters* [59].

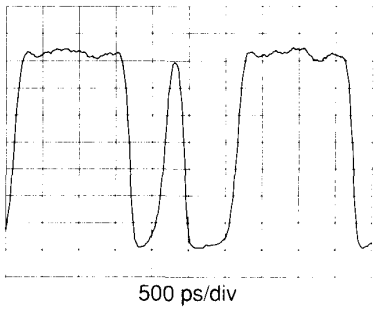

Fig. 28. Serial output waveform of a 2.7 GHz, 8 bit multiplexer-demultiplexer [57] measured by electrooptic sampling. The output word is 11110100.

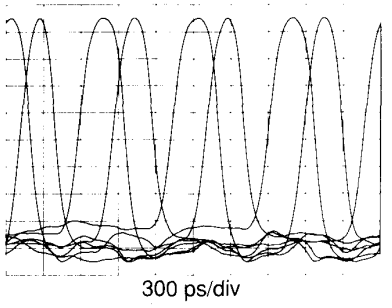

Fig. 29. 8-phase clock waveforms in 2.7 GHz multiplexer. An asymmetrical 2.7 GHz clock input results in timing skew in the 8-phase counter. The clock lines are 3 μm in width spaced 6 μm apart.

The electrooptic sampler directly measures voltages, but not currents, preventing a direct measure of 2-port parameters. Measuring the voltage as a function of position with the optical probe [60], similar to a slotted-line measurement, permits calculation of the incident and reverse waves on the transmission lines connecting to devices. From this information the network scattering parameters can then be determined.

The vector voltage due to the sum of the forward and reverse traveling waves on a lossless transmission line conductor is

$$V(z) = V^{+} \exp(-j\beta z) + V^{-} \exp(+j\beta z) \quad (33)$$

where V^{+} and V^{-} are the forward and reverse traveling wave coefficients, β is the wavenumber $2\pi/\lambda$, and z is the position. The traveling-wave coefficients are calculated by measuring this vector voltage as a function of position along a conductor using the optical probe then solving for these coefficients. For a one-port transmission line the ratio of the traveling wave coefficients V^{+} and V^{-} is the reflection coefficient Γ, or S_{11}, the return loss. An example of such a measured vector standing wave and the calculated reflection coefficient for an unterminated CPW transmission line at a drive frequency of 40 GHz is shown in Fig. 30, and a similar measurement with an unmatched load terminating the line at 20 GHz is shown in Fig. 31. Extending this technique to calculate the incident and reflected waves on the input and output ports of a

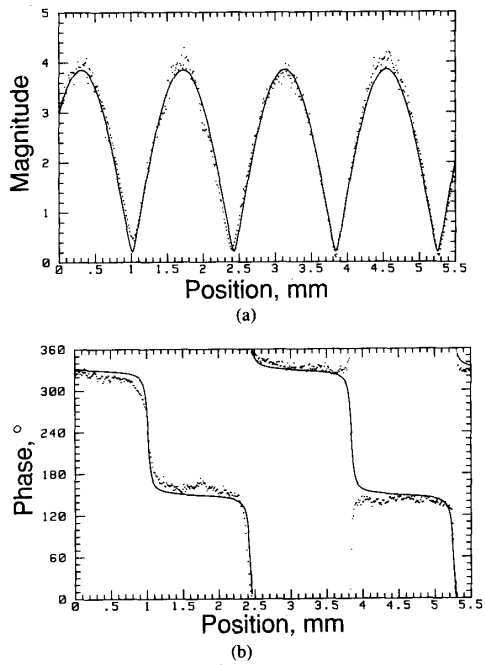

Fig. 30. (a) Magnitude and (b) phase of a 40 GHz voltage standing wave on an open-terminated GaAs coplanar waveguide transmission line. The points are the data and the solid line is the fitted curve. From this measurement a reflection coefficient of 0.90 at 80° is calculated. Each division of 10° in phase corresponds to 0.7 ps in time.

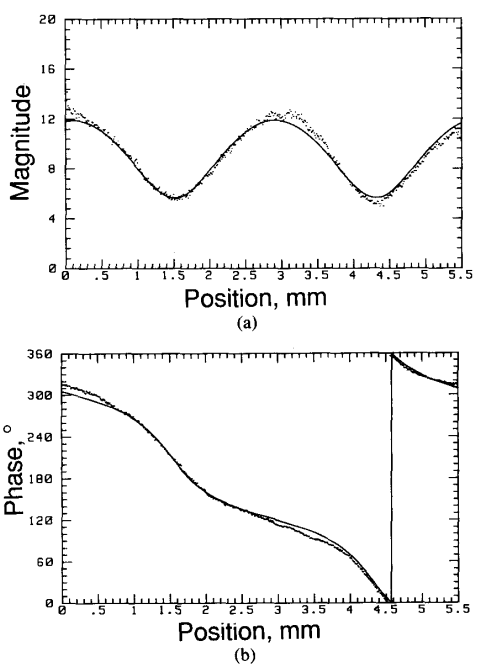

Fig. 31. (a) Magnitude and (b) phase of a 20 GHz voltage standing wave on a GaAs coplanar waveguide transmission line with a mismatched termination. The points are the data and the solid line is the fitted curve. From this measurement a reflection coefficient of 0.35 at 15° is calculated.

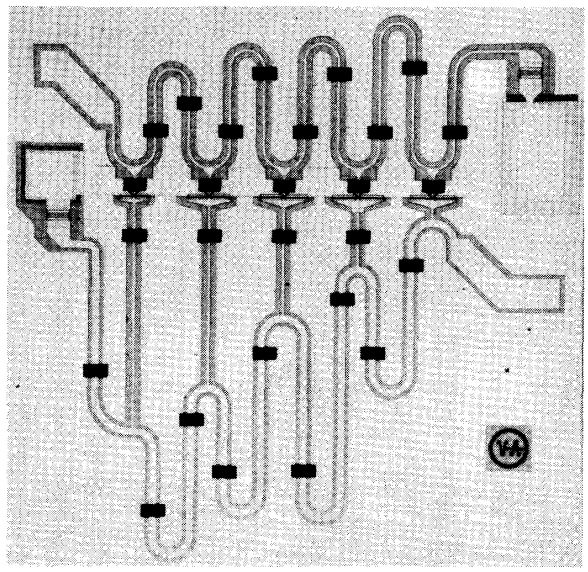

Fig. 32. Traveling-wave amplifier using coplanar waveguide transmission-line interconnects [62]. Photo courtesy of M. Riaziat, Varian Research Center.

network allows for calculation of the *S*-parameters with a reference plane defined *on* the integrated circuit.

On GaAs microwave amplifiers and similar MMIC's, the propagation of microwave signals internal to the circuit can be measured. Fig. 32 is a monolithic 2-18 GHz MESFET distributed amplifier from Varian Research Labs [61], [62] with coplanar-waveguide transmission line interconnects. The circuit diagram is shown in Fig. 33. In a distributed amplifier, a series of small transistors are connected at regular spacings between two high-impedance transmission lines. The high-impedance lines and the FET input and output capacitances together form synthetic transmission lines of 50 Ω characteristic impedance. Series stubs are used in the drain circuit, equalizing the phase velocities of the two lines and providing partial matching between the low impedance of the output line and the higher output impedances of the FET's at high frequencies, thereby peaking the gain. Measurements of interest include the relative drive levels to the individual FET's as influenced by the loss and cutoff frequency of the synthetic gate line, the small-signal voltage at the drain of each FET, and identification of the saturation mechanisms leading to amplifier gain compression.

Fig. 34 shows the small-signal gate voltages versus frequency for the amplifier of Fig. 32; several features can be noted. The rolloff beyond 18 GHz is the cutoff frequency of the periodically-loaded gate line, the slow rolloff with frequency is the gate line attenuation arising from the real part of the FET input admittance, and the ripples are standing waves resulting from mistermination of the gate line (i.e., the load resistance not equal to the synthetic line's characteristic impedance.)

Similar measurements can be made on MMIC's using microstrip transmission lines. Figs. 35 and 36 show the

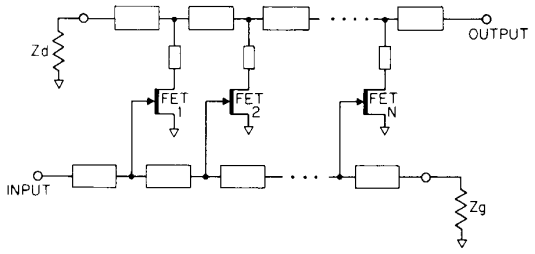

Fig. 33. Circuit diagram of distributed amplifier.

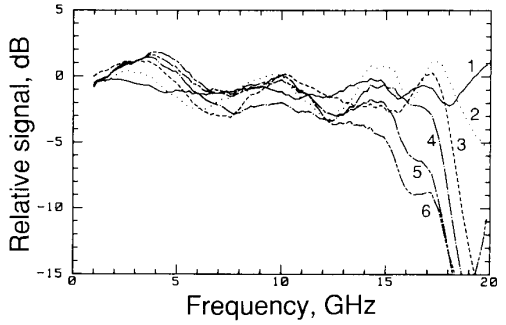

Fig. 34. Small-signal voltages at the five gates and at the gate line termination resistor in the coplanar 2–18 GHz distributed amplifier of Fig. 23. The line labeled 1 is the FET nearest the input, 2 is the next FET, and so on, until 6, which is the reverse termination.

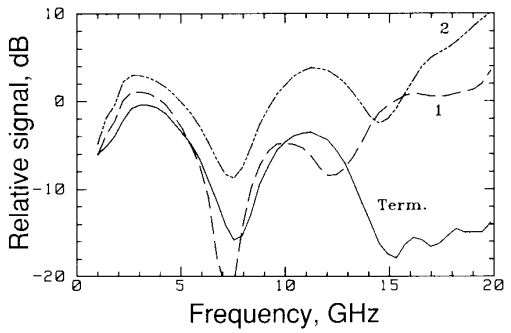

Fig. 35. Small-signal voltages at the first and second drains, and at the drain line reverse termination resistor, in a 2–18 GHz distributed amplifier using microstrip transmission lines [61].

small-signal drain voltages versus frequency for a distributed amplifier with microstrip transmission lines (Fig. 37, also from Varian Associates). The strong variation with frequency and position results from interference of the forward and reverse waves on the drain transmission line.

Used in the synchronous sampling mode, the electrooptic sampler can measure the voltage waveforms at internal nodes under conditions of circuit saturation, permitting identification of the saturation mechanisms. Fig. 38 shows the voltage waveforms at drains 4 and 5 of the microstrip distributed amplifier operating at 10 GHz and 7 dBm input power, corresponding to the 1 dB gain compression point. For this amplifier, at frequencies above 5 GHz, gain saturation arises predominantly from drain saturation (i.e., reduction of V_{dg} to the point where the drain end of

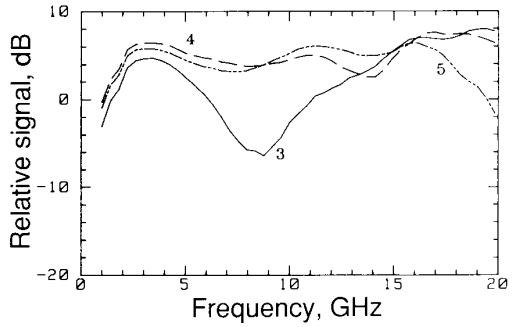

Fig. 36. Small-signal voltages at drains 3, 4, and 5 of the microstrip distributed amplifier.

the channel is no longer pinched off) of the fourth and fifth FET's. Saturation at drive frequencies as high as 21 GHz can be observed (Fig. 39). Even if the probed points had been accessible with electrical probes, these measurements would not be possible with sampling oscilloscopes (due to limited bandwidth), spectrum analyzers (magnitude response only), or network analyzers (small-signal response only).

V. Conclusion

A variety of new probing techniques for high-speed integrated circuits have been investigated by researchers, with the objective of providing an instrument with bandwidth greater than that of the tested device, a spatial resolution sufficient to permit access to finely spaced conductors within these circuits, measuring their potential independent of the potential of nearby conductors, and with negligible degradation of measurement accuracy from circuit perturbation. The techniques discussed in the introduction use either electron or optical beams to measure the electrical signals on an IC, and all have some degree of tradeoff between achieving best time resolution, spatial resolution, and perturbation of the circuit operation. Direct electrooptic sampling uses the substrate of the GaAs IC itself as the electrooptic modulator, eliminating external electrooptic elements and their invasive aspects, and permitting access to arbitrary points within the circuit without physical contact, to a resolution limited by the diameter of the focused infrared probe beam. With the substrate serving as the electrooptic element, the optical properties of the circuit must be considered (polishing of the substrate backside and metallization reflectivity), and probe beam absorption through deep levels in the GaAs substrate may affect circuit operation. Reducing the probe beam intensity or using a longer wavelength beam reduces this perturbation. The sections on system bandwidth and sensitivity describe limits on the instrument's time resolution and accuracy. Since the intensity modulations due to the electrooptic effect are small, full understanding of the noise sources in the system and methods for their suppression is crucial if the system is to provide useful circuit measurements. The system described in this paper has a potential time resolution of less than 2 ps, a corre-

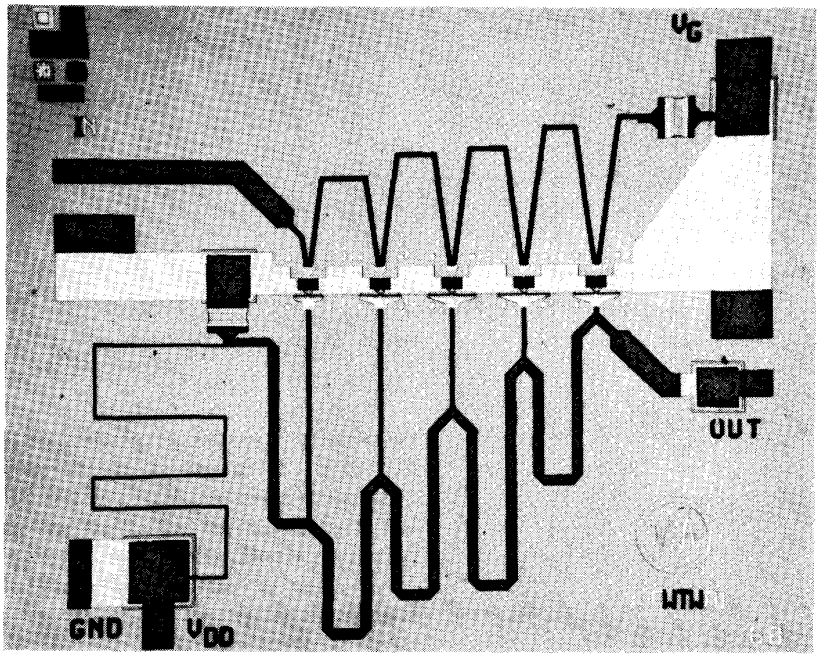

Fig. 37. Traveling-wave amplifier using microstrip transmission line interconnects [62]. Photo courtesy of R. LaRue, Varian Research Center.

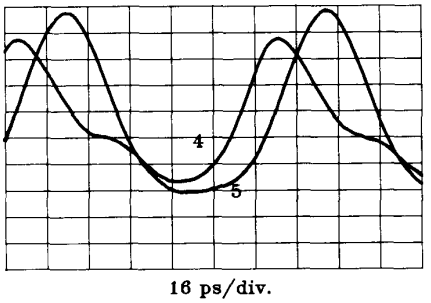

Fig. 38. Saturation at drains 4 and 5 of the microstrip distributed amplifier at 10 GHz and 7 dBm input power, the 1 dB gain compression point.

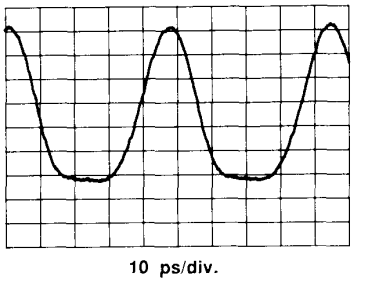

Fig. 39. Saturation at drain 3 of the microstrip distributed amplifier at 21 GHz drive frequency.

sponding bandwidth greater than 100 GHz, a working sensitivity of 70 $\mu V/\sqrt{Hz}$, and a spatial resolution of less than 3 microns.

The direct electrooptic sampling system has several aspects critical for IC testing in addition to internal node testing. Synchronization of the laser probe pulses to the signal generator driving the IC permits operation of the circuit in its normal fashion, driven by microwave or digital signals from electronic sources. Integration of the electrooptic sampling system with a microwave wafer probe station permits wafer-level optical probing of high-speed IC's. Measurement results on a variety of GaAs analog microwave and high-speed digital integrated circuits have been presented, such as gate propagation delay and logic timing measurements of an 8 bit multiplexer/demultiplexer clocked at 2.6 GHz, a 20 gate inverter chain using 1 μm MESFET technology, 18 GHz static frequency dividers using 0.2 μm MESFET technology on digital IC's, internal signal measurements on 2–18 GHz microstrip and coplanar waveguide traveling-wave amplifiers, and voltage standing wave and reflection coefficient measurements on transmission lines at frequencies to 40 GHz. Extending the standing-wave measurements to two-port devices will permit on-wafer millimeter-wave scattering parameter measurements with the reference planes located at the device terminals on the IC.

Acknowledgment

The authors thank J. F. Jensen of Hughes Research Laboratories, Malibu, CA, M. Riaziat of Varian Research Center, K. R. Gleason of Cascade Microtech and TriQuint Semiconductor, Inc., and S. Swierkowski of Lawrence Livermore National Labs for their assistance with the GaAs circuits. Thanks to T. Baer and J. D. Kafka of Spectra-Physics, Inc., for their assistance with the optical pulse compressor. We acknowledge the generous

equipment donations of Cascade Microtech, Inc., Tektronix, Inc., and the Hewlett-Packard Co.

REFERENCES

[1] H. Q. Tserng and B. Kim, "110 GHz GaAs FET Oscillator," *Electron. Lett.*, vol. 21, pp. 178-179, 1985.

[2] T. Henderson, M. I. Aksun, C. K. Peng, H. Morkoc, P. C. Chao, P. M. Smith, K-H. G. Duh, and L. F. Lester, "Microwave performance of a quarter-micrometer gate low-noise pseudomorphic InGaAs/AlGaAs modulation-doped field effect transistor," *IEEE Electron Device Lett.*, vol. EDL-7, pp. 649-651, 1986.

[3] T. C. L. G. Sollner, E. R. Brown, W. D. Goodhue, and H. Q. Le, "Observation of millimeter-wave oscillations from resonant tunneling diodes and some theoretical considerations of ultimate frequency limits," *Appl. Phys. Lett.*, vol. 50, pp. 332-334, 1987.

[4] J. F. Jensen, L. G. Salmon, D. S. Deakin, and M. J. Delaney, "Ultra-high speed GaAs static frequency dividers," *Tech. Dig. 1986 Int. Electron Device Meet.*, 1986, p. 476-479.

[5] E. W. Strid, K. R. Gleason, and T. M. Reeders, "On-wafer measurement of gigahertz integrated circuits," in *VLSI Electronics: Microstructure Science*, Vol. 11. New York: Academic, 1985, pp. 265-287.

[6] Cascade Microtech, Inc., P. O. Box 2015, Beaverton, OR 97075.

[7] Hypres, Inc., 175 Clearbrook Rd., Elmsford, NY 10523.

[8] "Electron-beam testing of VLSI chips gets practical," *Electronics*, pp. 51-54, Mar. 24, 1986.

[9] R. Iscoff, "E-beam probing systems: Filling the submicron gap," *Semiconductor Int.*, pp. 62-68, Sept. 1985.

[10] P. May, J.-M. Halbout, and G. Chiu, "Laser pulsed E-beam system for high speed IC testing," in *Picosecond Electronics and Optoelectronics*. New York: Springer-Verlag, 1987.

[11] R. B. Marcus, A. M. Weiner, J. H. Abeles, and P. S. D. Lin, "High-speed electrical sampling by fs photoemission," *Appl. Phys. Lett.*, vol. 49, pp. 357-359, 1986.

[12] J. Bokor, A. M. Johnson, R. H. Storz, and W. M. Simpson: "High-speed circuit measurements using photoemission sampling," *Appl. Phys. Lett.*, vol. 49, pp. 226-228, 1986.

[13] A. M. Weiner, R. B. Marcus, P. S. D. Lin, and J. H. Abeles, "Photoemissive testing of high-speed electrical waveforms," in *Picosecond Electronics and Optoelectronics*. New York: Springer-Verlag, 1987.

[14] H. K. Heinrich, D. M. Bloom, and B. R. Hemenway, "Noninvasive sheet charge density probe for integrated silicon devices," *Appl. Phys. Lett.*, vol. 48, pp. 1066-1068, 1986.

[15] H. K. Heinrich, B. R. Hemenway, K. A. McGroddy, and D. M. Bloom, "Measurement of real-time digital signals in a silicon bipolar junction transistor using a noninvasive optical probe," *Electron. Lett.*, vol. 22, pp. 650-652, 1986.

[16] J. A. Valdmanis, G. A. Mourou, and C. W. Gabel, "Picosecond electro-optic sampling system," *Appl. Phys. Lett.*, vol. 41, pp. 211-212, 1982.

[17] B. H. Kolner, D. M. Bloom, and P. S. Cross, "Electro-optic sampling with picosecond resolution," *Electron. Lett.*, vol. 19, 574-575, 1983.

[18] J. A. Valdmanis, G. A. Mourou, and C. W. Gabel, "Subpicosecond electrical sampling," *IEEE J. Quantum Electron.*, vol. QE-19, pp. 664-667, 1983.

[19] J. A. Valdmanis and G. Mourou, "Subpicosecond electrooptic sampling: Principles and applications," *IEEE J. Quantum Electron.*, vol. QE-22, pp. 69-78, 1986.

[20] D. R. Dykaar, R. Sobolewski, J. F. Whitaker, T. Y. Hsiang, G. A. Mourou, M. A. Hollis, B. J. Clifton, K. B. Nichols, C. O. Bozler, and R. A. Murphy, "Picosecond characterization of ultrafast phenomena: New device and new techniques," in *Ultrafast Phenomena V*, G. R. Fleming and A. E. Siegman, Eds. New York: Springer-Verlag, 1986, pp. 103-106, Springer Ser. Chem. Phys., vol. 46.

[21] J. A. Valdmanis and S. S. Pei, "A non-contact picosecond prober for integrated circuit testing," in *Picosecond Electronics and Optoelectronics*. New York: Springer-Verlag, 1987.

[22] ——, "Picosecond non-contact electrooptic probing for integrated circuits," *Tech. Dig. CLEO'87*, 1987, pp. 352-353.

[23] J. A. Valdmanis, Presentation FN3 at CLEO'87 and private communication.

[24] I. P. Kaminow, *An Introduction to Electro-Optic Devices*. New York: Academic, 1974.

[25] I. P. Kaminow and E. H. Turner, "Electrooptic light modulators," *Proc. IEEE*, vol. 54, pp. 1374-1390, 1966.

[26] B. H. Kolner and D. M. Bloom, "Direct electrooptic sampling of transmission-line signals propagating on a GaAs substrate," *Electron. Lett.*, vol. 20, pp. 818-819, 1984.

[27] ——, "Electrooptic sampling in GaAs integrated circuits," *IEEE J. Quantum Electron.*, vol. QE-22, pp. 79-93, 1986.

[28] A. Yariv and P. Yeh, *Optical Waves in Crystals*. New York: Wiley, 1984, pp. 286-287.

[29] ——, *Optical Waves in Crystals*. New York: Wiley, 1984, p. 230.

[30] J. L. Freeman, S. K. Diamond, H. Fong, and D. M. Bloom, "Electrooptic sampling of planar digital integrated circuits," *Appl. Phys. Lett.*, vol. 47, pp. 1083-1084, 1985.

[31] W. H. Knox, R. L. Fork, M. C. Downer, R. H. Stolen, and C. V. Shank, "Optical pulse compression to 8 fs at a 5-kHz repetition rate," *Appl. Phys. Lett.*, vol. 46, pp. 1120-1121, 1985.

[32] C. H. Brito-Cruz, R. L. Fork, and C. V. Shank, "Compression of optical pulses to 6 fs using cubic phase distortion compensation," *Tech. Dig. CLEO'87*, 1987, pp. 12-13.

[33] A. S. Gouveia-Neto, A. S. L. Gomes, and J. R. Taylor, "Generation of 33-fsec pulses at 1.32 μm through a high-order soliton effect in a single-mode optical fiber," *Opt. Lett.*, vol. 12, pp. 395-397, 1987.

[34] B. Zysset, W. Hodel, P. Beaud, and H. P. Weber, "200-femtosecond pulses at 1.06 μm generated with a double-stage pulse compressor," *Opt. Lett.*, vol. 11, pp. 156-158, 1986.

[35] R. N. Bracewell, *The Fourier Transforms and its Applications*. New York: McGraw-Hill, 1978.

[36] D. Cotter, "Technique for highly stable active mode-locking," in *Ultrafast Phenomena IV*, D. A. Auston and K. B. Eisenthal, Eds. New York: Springer-Verlag, 1984, pp. 78-80.

[37] M. J. W. Rodwell, K. J. Weingarten, D. M. Bloom, T. Baer, and B. H. Kolner: "Reduction of timing fluctuations in a mode-locked Nd:YAG laser by electronic feedback," *Opt. Lett.*, vol. 11, pp. 638-640, 1986.

[38] E. B. Treacy, "Optical pulse compression with diffraction gratings," *IEEE J. Quantum Electron.*, vol. QE-5, pp. 454-458, 1969.

[39] D. Grischkowsky and A. C. Balant, "Optical pulse compression based on enhanced frequency chirping," *Appl. Phys. Lett.*, vol. 41, pp. 1-3, 1982.

[40] J. D. Kafka, B. H. Kolner, T. Baer, and D. M. Bloom, "Compression of pulses from a continuous-wave mode-locked Nd:YAG laser," *Opt. Lett.*, vol. 9, pp. 505-506, 1984.

[41] A. J. Taylor, J. M. Wiesenfeld, G. Eisenstein, R. S. Tucker, J. R. Talman, and U. Koren, "Electrooptic sampling of fast electrical signals using an InGaAsP injection laser," *Electron. Lett.*, vol. 22, pp. 61-62, 1986.

[42] A. J. Taylor, J. M Wiesenfeld, R. S. Tucker, G. Eisenstein, J. R. Talman, and U. Koren, "Measurement of a very high-speed InGaAs photodiode using electrooptic sampling," *Electron. Lett.*, vol. 22, pp. 325-327, 1986.

[43] J. M. Wiesenfeld, R. S. Tucker, A. Antreasyan, C. A. Burrus, and A. J. Taylor, "Electrooptic sampling measurements of high-speed InP integrated circuits," *Appl. Phys. Lett.*, vol. 50, pp. 1310-1312, 1987.

[44] J. P. Heritage, R. N. Thurston, W. J. Tomlinson, and A. M. Weiner, "Spectral windowing of frequency-modulated optical pulses in a grating compressor," *Appl. Phys. Lett.*, vol. 47, pp. 87-89, 1985.

[45] N. J. Halas and D. Grischkowsky, "Simultaneous optical pulse compression and wing reduction," *Appl. Phys. Lett.*, vol. 48, pp. 823-825, 1986.

[46] M. J. W. Rodwell, K. J. Weingarten, J. L. Freeman, and D. M. Bloom, "Gate propagation delay and logic timing of GaAs integrated circuits measured by electro-optic sampling," *Electron. Lett.*, vol. 22, pp. 499-501, 1986.

[47] J. D. Kafka and T. Baer, "Intensity fluctuations in optical pulse compression," in *Tech. Dig. CLEO'87*, 1987, pp. 276-277.

[48] K. J. Weingarten, M. J. W. Rodwell, and D. M. Bloom, "Picosecond sampling of GaAs integrated circuits," in *Picosecond Electronics and Optoelectronics*. New York: Springer-Verlag, 1987.

[49] M. N. Islam, L. F. Mollenauer, and R. H. Stolen, in *Ultrafast Phenomena V*, G. R. Fleming and A. E. Siegman, Eds. New York: Springer-Verlag, 1986, pp. 46-50, Springer Ser. Chem. Phys., vol. 46.

[50] J. D. Kafka and T. Baer, "Fiber Raman soliton laser pumped by a Nd:YAG laser," *Opt. Lett.*, vol. 12, pp. 181-183, 1987.

[51] R. M. Shelby, M. D. Levenson, and P. W. Bayer, "Guided acoustic-

wave Brillouin scattering," *Phys. Rev. B*, vol. 31, pp. 5244–5252, 1985.
[52] G. M. Martin, "Optical assessment of the main electron trap in bulk-semi-insulating GaAs," *Appl. Phys. Lett.*, vol. 39, pp. 747–748, 1981.
[53] P. Dobrilla and J. S. Blakemore, "Experimental requirements for quantitative mapping midgap flaw concentration in semi-insulating GaAs wafers by measurements of near-infrared transmittance," *J. Appl. Phys.*, vol. 58, pp. 208–218, 1985.
[54] S. Swierkowski, K. Mayeda, and C. McGonaghy, "A sub-200 picosecond GaAs sample-and-hold circuit for a multi-gigasample/second integrated circuit," *Tech. Dig. 1985 Int. Electron Devices Meet.*, 1985, pp. 272–275.
[55] X.-C. Zhang and R. K. Jain: "Measurement of on-chip waveforms and pulse propagation in digital GaAs integrated circuits by picosecond electro-optic sampling," *Electron. Lett.*, vol. 22, pp. 264–265, 1986.
[56] J. F. Jensen, K. J. Weingarten, and D. M. Bloom, in *Picosecond Electronics and Optoelectronics*. New York: Springer-Verlag, 1987.
[57] G. D. McCormack, A. G. Rode, and E. W. Strid, "A GaAs MSI 8-bit multiplexer and demultiplexer," in *Proc. 1982 GaAs IC Symp.*, 1982, pp. 25–28.
[58] X.-C. Zhang, R. K. Jain, and R. M. Hickling, "Electrooptic sampling analysis of timing patterns at critical internal nodes in Gigabit GaAs multiplexers/demultiplexers," in *Picosecond Electronics and Optoelectronics*. New York: Springer-Verlag, 1987.
[59] R. E. Collins, *Foundations of Microwave Engineering*. New York: McGraw-Hill, 1966.
[60] K. J. Weingarten, M. J. W. Rodwell, J. L. Freeman, S. K. Diamond, and D. M. Bloom, "Electrooptic sampling of gallium arsenide integrated circuits," in *Ultrafast Phenomena V*, G. R. Fleming and A. E. Siegman, Eds. New York: Springer-Verlag, 1986, p. 98, Springer Ser. Chem. Phys., vol. 46.
[61] M. J. W. Rodwell, M. Riaziat, K. J. Weingarten, B. A. Auld, and D. M. Bloom, "Internal microwave propagation and distortion characteristics of travelling-wave amplifiers studied by electro-optic sampling," *IEEE Trans. Microwave Theory Tech.*, vol. MTT-34, pp. 1356–1362, 1986.
[62] G. Zdasiuk, M. Riaziat, R. LaRue, C. Yuen, and S. Bandy, "Enhanced performance ultrabroadband distributed amplifiers," in *Picosecond Electronics and Optoelectronics*. New York: Springer-Verlag, 1987.

Kurt J. Weingarten (S'82) was born January 30, 1961, in St. Petersburg, FL. He received the B.S. degree in electrical engineering from the Georgia Institute of Technology, Atlanta, in 1983, and the M.S. degree in electrical engineering from Stanford University, Stanford, CA, in 1985.

He is currently a Ph.D. candidate in electrical engineering and works as a Research Assistant in the Edward L. Ginzton Laboratory, W. W. Hansen Laboratories of Physics, Stanford University. His research interests are electrooptic sampling of GaAs IC's, high-speed electronic testing, and ultrafast optical pulse generation.

Mr. Weingarten is a student member of the Optical Society of America.

Mark Rodwell was born on January 18, 1960, in Altrincham, England. He received the B.S. degree in electrical engineering from the University of Tennessee, Knoxville, in 1980, and the M.S.E.E. degree from Stanford University, Stanford, in 1982.

Currently, he is a Ph.D. candidate in electrical engineering at Stanford, pursuing research in picosecond electronics and optoelectronics. From 1982 through 1984, he worked at AT&T Bell Laboratories, designing fiber-optic digital transmission systems.

David M. Bloom (S'68–M'76–M'80–SM'86–F'87) was born on October 10, 1948, in Brooklyn, NY. He received the B.S. degree in electrical engineering from the University of California, Santa Barbara, in 1970, and the M.S. and the Ph.D. degrees in electrical engineering from Stanford University, Stanford, CA, in 1972 and 1975, respectively.

From 1975 to 1977 he was employed by Stanford University as a Research Associate. During this period he was awarded an IBM Postdoctoral Fellowship. From 1977 to 1979 he was employed by Bell Telephone Laboratories, Holmdel, NJ, where he conducted research on optical phase conjugation, ultrafast optical pulse propagation in fibers, and tunable color-center lasers. From 1979 to 1983 he served on the staff and later as a Project Manager at Hewlett-Packard Laboratories, Palo Alto, CA. While there he conducted and managed research on fiber optical devices, high-speed photodetectors, and picosecond electronic measurement techniques. In late 1983 he joined the Edward L. Ginzton Laboratory, W. W. Hansen Laboratories of Physics, Stanford University, where he is currently an Associate Professor of Electrical Engineering. His current research interests are ultrafast optics and electronics.

Dr. Bloom was awarded the 1980 Adolph Lomb Medal of the Optical Society of America for his pioneering work on the use of nonlinear optical processes to achieve real-time conjugate wavefront generation. In 1981 he was elected a Fellow of the Optical Society of America in recognition of his distinguished service in the advancement of optics. He was the IEEE LEOS Traveling Lecturer for 1985 and in 1986 was elected a Fellow of the IEEE for contributions to nonlinear optics and ultrafast optoelectronics.